Si Based Magnetic Semiconductors 14

John F. DiTusa

Contents

Introduction: Why Spintronics in Silicon? 524
Attempts to Make Silicon- and Germanium-Based Magnetic Semiconductors 527
  Transition Metal Dopants in Crystalline Silicon 527
  Transition Metal Doping of Crystalline Germanium 531
  Transition Metal Doping of Amorphous Silicon and Germanium 537
Magnetic Silicides and Germanides 539
  Monosilicides and Monogermanides 542
Dilute SiC-Based Magnetic Semiconductors 550
Summary and Concluding Remarks 551
Directions for Future Research 551
References 552
Further Reading 560

Abstract

The efforts over the past decade to identify and characterize magnetic semiconducting systems that would be compatible with present-day silicon technologies are reviewed. Investigations that have explored transition metal doping of the group IV semiconductors silicon and germanium are discussed along with intermetallic compounds such as silicides and germanides that may play the role of a magnetic semiconducting source of polarized electrons. Thin films and nanostructures of these materials have been grown by a number of synthesis techniques, and the resulting structural properties, including the important issue of homogeneity of dopants, are critically surveyed. The resulting magnetic and carrier transport properties are also reviewed.

J.F. DiTusa (✉)
Department of Physics and Astronomy, Louisiana State University, Baton Rouge, LA, USA
e-mail: ditusa@phys.lsu.edu

© Springer Science+Business Media Dordrecht 2016

Y. Xu et al. (eds.), *Handbook of Spintronics*,
DOI 10.1007/978-94-007-6892-5_21

List of Abbreviations

AFM	Antiferromagnetic
CVD	Chemical vapor deposition
FC	Field cooled
FM	Ferromagnetic
HM	Helimagnetic
HRTEM	High-resolution transmission electron microscopy
MBE	Molecular beam epitaxy
MFM	Magnetic force microscopy
PLD	Pulsed laser deposition
RDE	Reactive deposition epitaxy
SPE	Solid-phase epitaxy
SQUID	Superconducting quantum interference device
STEM	Scanning transmission electron microscopy
STM	Scanning tunneling microscopy
T_c	Curie temperature
TEM	Transmission electron microscopy
TM	Transition metal
XRD	X-ray diffraction
ZFC	Zero field cooled
α	Amorphous
μ_B	Bohr magneton
ρ	Resistivity

Introduction: Why Spintronics in Silicon?

From a historical perspective, the advances made over the past 60 years in the materials science of silicon and the resulting device design using silicon as a central semiconductor are truly exceptional. The result of this enormous success is that Si is now deeply entrenched as the choice semiconductor in almost all electronic technologies. Its importance is reflected in the fact that it captures an impressive 90 % of the semiconductor market as the associated industries continue to invest large sums of money and time to develop silicon device fabrication. It is reasonable to expect then that making new technologies compatible with silicon will vastly reduce the time and investment necessary to bring them to market. Presumably, this holds true for the case of the developing technology of spintronics.

However, silicon also has its limitations as a semiconductor and discovering materials, and methods for implementing new spintronics ideas into a silicon-based technology have proved to be extraordinarily challenging. In this chapter, I outline these challenges and the progress that has been made to overcome them, highlighting some of the creative ideas that are being pursued. In particular, I emphasize the explorations of magnetic semiconducting materials that are necessary to implement spintronics on a silicon-based platform.

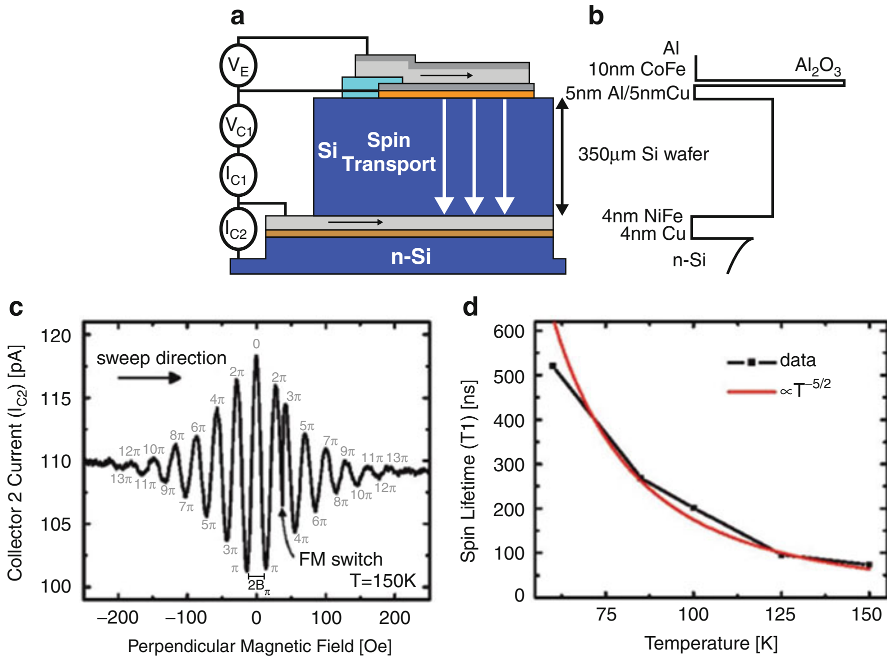

Fig. 1 Coherent spin transport in silicon. (**a**) Schematic view and (**b**) associated conduction band diagram for the silicon spin transport device employed in Ref. [3]. (**c**) Spin precession and dephasing effect (Hanle effect) of Si conduction band electrons. (**d**) Experimental spin lifetimes (Reprinted figures with permission from Huang et al. [3]. Copyright (2007) by the American Physical Society)

One of the great advantages of using silicon as a base material for polarized current and, perhaps, spin current transport is that spin relaxation lifetimes are predicted [1] and observed [2–4] to be very long in Si. The very weak spin-orbit coupling in crystalline silicon means that spin relaxation may be as much as 10^5 times as long as the elastic scattering times that determine charge conductivities. Because of this long relaxation time, the control and detection of spin currents on the length and time scales of technological interest is a distinct possibility. Simple analyses of conduction electron spin resonance measurements in phosphorus-doped Si (*n*-type) performed decades ago [5–11] demonstrated a spin relaxation time of 10 ns near room temperature that is relatively insensitive to the doping level across the metal-insulator transition [12]. More recently transport experiments, spin valve, and Hanle-type spin precession experiments in very clean silicon samples show coherent spin transport over length scales as long as 350 μm at 85 K [2–4] (Fig. 1) and extend in lateral devices to over 2 mm at 50 K [3]. These latter experiments employed $Co_{84}Fe_{16}$ ferromagnetic films to inject a spin-polarized current via tunneling across a thin Al_2O_3 insulating layer into a nonmagnetic thin film anode (Al and Cu). The carriers are given sufficient energy by the tunnel junction voltage

to travel ballistically in the nonmagnetic thin film and then to cross over the Schottky barrier into the Si conduction band. $Ni_{80}Fe_{20}$ ferromagnetic films are employed for polarized current detection [13, 14]. The corresponding relaxation time of about 500 ns (at 60 K) and the demonstration of spin transport at temperatures as high as 260 K [15] provide optimism that the logic and memory functions envisioned for spintronics can be accomplished on a silicon platform. These measured relaxation times can be compared with the time-resolved Faraday rotation experiments in n-type GaAs, revealing a spin coherence time of 200 ns at 4 K which is reduced to 1 ns at 100 K [16]. The striking conclusion is that if the challenges of producing and detecting spin currents in silicon-based devices can be overcome, this semiconductor may be far superior to any others for implementing spin-dependent technologies. However, the fact that that silicon is not a direct bandgap semiconductor means that the detection and control of spin currents will likely not be accomplished optically. This may be a severely limiting fact for many envisioned applications.

Since optical means of spin current production in silicon is likely unrealistic, effective means of injecting spin-polarized currents from itinerant magnets take on greater importance. Unfortunately, spin-polarized current injection into Si from magnetic materials is just as difficult as in other semiconductors. Itinerant ferromagnetism occurs most readily in materials with large electronic density of states at the Fermi level which typically translates into high carrier density metals. Prototypical itinerant magnets such as the elemental systems iron, cobalt and nickel, and the alloys formed by combining them all have reasonably metallic carrier densities. Thus, there is a typically large band mismatch at the interface between these metals and semiconductors resulting in high Schottky barriers. The consequence is a large resistance to currents at the interfaces between the source of a spin-polarized current and the semiconductor which effectively limits the injected current density. Increasing the dopant density in the semiconductor in an effort to reduce the Schottky barrier heights tends to increase carrier scattering, further reducing the polarization of the injected current. The challenge then is to find magnetic materials with high Curie temperatures that tend to form high-quality Ohmic contacts to silicon with low interface scattering. In addition, it is likely important that the conductivities of the magnetic materials and the semiconductor be similar in order to avoid any conductivity mismatch problems [17]. Discovering solutions to these problems, or finding ways around them, is necessary for progress toward active spintronics elements.

To set the scale of the problem of compatibility of ferromagnetic metals with silicon, I list a few quantitative examples of Schottky barrier heights. For common transition metal ferromagnets, such as $Co_{1-x}Fe_x$ and NiFe or Ni films on Si [18–20], Schottky barrier heights are usually between 0.6 and 0.73 eV. Some silicide systems can have smaller barriers as was demonstrated for MnSi/Si nanowire devices where a 0.1 eV barrier was measured [21]. A systematic investigation of Schottky barrier heights of silicon/metallic boundaries can be found in Ref. [22] where Uhrmann et al. measure the changes in effective barrier heights between CoFe, CoFeB, and NiFe alloys with annealing temperature, dopant density, and inclusion of MgO tunneling barriers. They observed a ~0.65 eV barrier

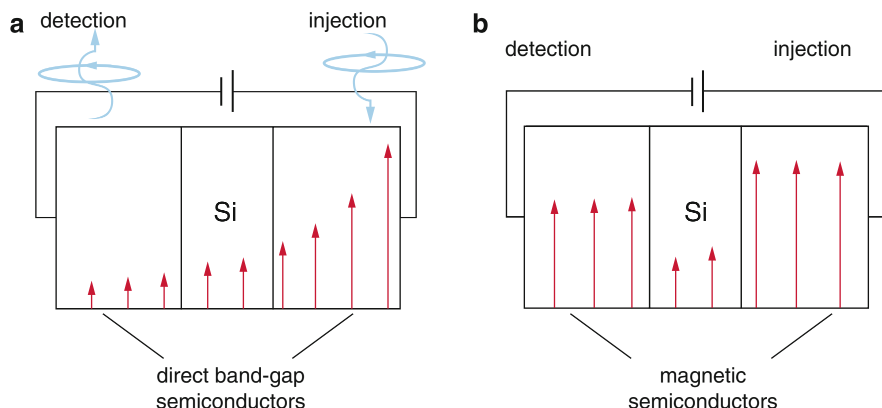

Fig. 2 Proposed schemes for spin injection and detection in silicon. (**a**) Optical scheme based upon optical processes in direct bandgap semiconductors surrounding silicon. (**b**) Electrical scheme using magnetic semiconducting materials (Reprinted figure with permission from Zutic et al. [25]. Copyright (2006) by the American Physical Society)

nearly independent of the identity of the metallic ferromagnetic film. However, they found that they could reduce barrier height by ~20 % by increasing the doping density in the Si from 10^{15} to 10^{18} cm^{-3}. Another method for reducing Schottky barrier heights is to employ low work function metals. This method has been used to demonstrate spin-polarized tunneling from $Ni_{80}Fe_{20}$ into Si through an Al_2O_3 tunnel barrier where the inclusion of low work function metals Gd and Yb reduced the effective Schottky barriers [23, 24]. Surprisingly, the Gd tended not to disturb the carrier polarization, while 2 nm thickness of Yb suppressed it [23, 24].

The most obvious avenue to effectively reduce Schottky barrier heights, band matching to the semiconductor by employing magnetic semiconductors for the ferromagnetic components of spintronic devices, is the subject of much investigation. However, a magnetic semiconductor with a large Curie temperature that is compatible with silicon technology, including the ability to form high-quality interfaces with Si, has not been discovered [25]. If appropriate materials can be identified, models suggest that detection and injection of polarized currents using currently available techniques should indeed be possible [26] (see Fig. 2).

Attempts to Make Silicon- and Germanium-Based Magnetic Semiconductors

Transition Metal Dopants in Crystalline Silicon

There are several avenues that have been explored for producing silicon-based magnetic semiconductors. Following the successful demonstration of Mn doping of GaAs for producing a magnetic semiconductor with moderate Curie temperatures (up to 180 K [27, 28]), a number of attempts to produce similar results in transition

metal doping of Si were made. Included were attempts at Mn doping for exactly the same reason it was attempted in the III–V semiconductors; Mn ions tend to be in a high spin state (spin 5/2 is typical for Mn^{2+}). Early experimental investigations employing sputtering, ion implantation, and molecular beam epitaxy (MBE) techniques for synthesizing thin films of Mn-doped Si were promising [29–32]. For example, 5 % Mn-doped Si films synthesized by sputtering with a subsequent high-temperature anneal displayed two Curie temperatures, one at 50 K and another above 250 K [29]. Since the XRD patterns displayed only Si peaks, with a shift of the diffraction pattern indicating an expanded lattice constant, the authors concluded that they had achieved Mn doping of Si. A second method was to ion implant Mn into silicon since nonequilibrium dopant concentrations can typically be achieved through these methods [30]. Again, high Curie temperatures were reported with an enhanced magnetic signal observed with an increasing sample annealing temperature. However, for an annealing temperature of 800 °C, a decreased magnetic signal was observed that corresponded to a measured diffusion of Mn out of the samples.

Unfortunately, more sophisticated investigations into films of this type revealed that the Mn dopants may not be truly incorporated into the Si structure. Nanoprecipitates with a typical diameter of 5 nm were routinely detected [33, 34] (see Fig. 3). Electron microscopy [34] and synchrotron X-ray diffraction [35, 36] observed the presence of higher Mn silicide precipitates which are usually referred to under the moniker $MnSi_{1.7}$. The films produced via MBE methods were investigated by X-ray diffraction and X-ray absorption which also revealed evidence for this same phase along with little to suggest that Mn was incorporated into the Si structure [31]. These experiments indicate that, as one might expect, Mn is difficult to dope into Si. This conclusion is compatible with the fact that transition metals have very low solubility in silicon so that second phases frequently nucleate at very low densities. For example, the solubility limit of Mn in crystalline Si is only about 10^{-16} cm^{-3} at 1,000 °C [37]. This low solubility limit makes the creation of a FM semiconductor by chemical substitution of Mn for Si impossible under equilibrium conditions and highly unlikely even for nonequilibrium-synthesized samples.

The overall picture remains somewhat confusing. It appears that a consensus has been forming that the magnetism found in the Mn-doped Si materials results mainly from second phases, mostly $MnSi_{1.7}$, forming nanoscopic clusters. However, there are many unanswered questions related to this consensus. First, the compounds referred to as $MnSi_{1.7}$ are not a single entity, but a set of closely related compounds having stoichiometries between $MnSi_{1.67}$ and $MnSi_{1.75}$. These form in a crystal structure known as Nowotny chimney ladder phases and include the compounds Mn_4Si_7, $Mn_{11}Si_{19}$, $Mn_{15}Si_{26}$, and $Mn_{27}Si_{47}$ [38]. Growing a sample that contains only a single one of these compounds is difficult which leaves much uncertainty in the characterization of their physical properties. In addition, these compounds are thought to be self-doped semiconductors with a bandgap of ~0.6 eV. Based on this identification, several recent investigations suggest that thin film and nanowire samples of $MnSi_{1.7}$ have promise as thermoelectric materials [39, 40]. In contrast, bulk samples of Mn_4Si_7 typically display fairly robust metallic behavior below

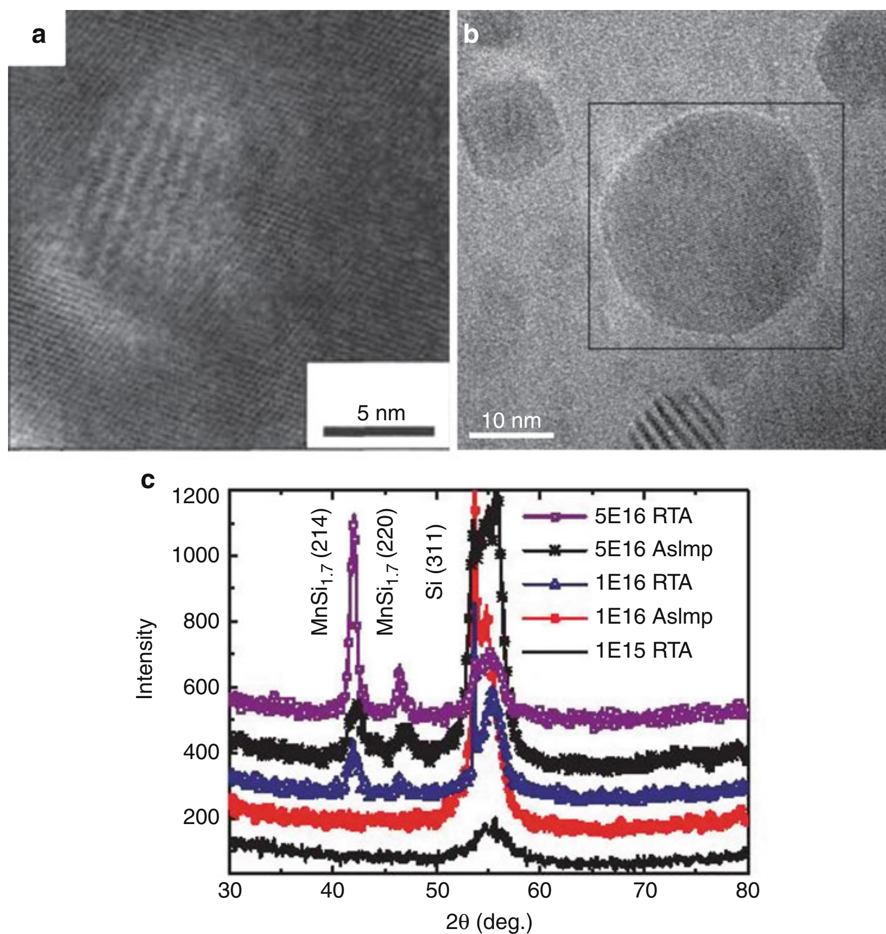

Fig. 3 Ion implantation of Mn in Si: example of a nanoprecipitate formation, likely $MnSi_{1.7}$ phase. (**a**) HRTEM image (Reprinted with permission from Awo-Affouda et al. [33]. Copyright (2006), American Vacuum Society). (**b**) High-resolution TEM. (**c**) X-ray diffraction grazing incidence scans of Mn-implanted Si (Reprinted figures (**b**, **c**) with permission from Zhou et al. [34]. Copyright (2007) by the American Physical Society)

room temperature including residual resistivity ratios, ρ(300 K)/ρ(4 K), of several hundred indicating long mean free paths for the carriers at low temperature [41]. The magnetic properties of Mn_4Si_7 are also somewhat confusing. Ferromagnetism has been observed below $T_c = 47$ K with an extraordinarily small magnetic moment (0.012 μ_B) which evolves to a Curie-Weiss-like behavior characterized by a fluctuating magnetic moment of 0.3 μ_B [41] above T_c. The conclusion from these measurements is that Mn_4Si_7 is a weak itinerant ferromagnet. This idea is somewhat difficult to reconcile with the thought that these compounds are self-doped semiconductors, except if the doping is responsible for both the large conduction and the

magnetism observed in these compounds. More importantly, the low Curie temperatures exhibited by the bulk samples of these compounds make the identification of these phases as the responsible precipitates for the high Curie temperatures found in the attempted Mn-doped Si films more than a little suspect.

It appears that Mn doping of silicon has not been convincingly demonstrated, but that the cause of magnetic behavior observed is not known, particularly in light of the realization that likely precipitates have low Curie temperatures in bulk samples. Thus, the origin of the high Curie temperatures observed in sputtered and ion-implanted films remains an open question [42]. In addition, whether materials with magnetic precipitates could be useful for producing polarized spin currents continues to be questioned in the literature. In fact, some view the low solubility of transition metals in Si as advantageous for the growth of nanoparticles in silicon matrix [43].

Despite the less-than-satisfying picture presented above for transition metal doping of Si as a route to ferromagnetic semiconductors, there are several new ideas stemming from theoretical work that lend some optimism to future investigations. One investigation indicates that interstitial dopant sites are typically preferred over substitutional ones [44]; however, the application of pressure may stabilize a substitutional site for Mn. Furthermore, this work indicates that Mn placed at interstitial sites tend to stabilize nearest neighbor substitutions which would be more favorable for the nucleation of ferromagnetism [29, 44]. A related idea is to include co-dopants along with Mn to increase the Mn solubility and stabilize the Mn in substitutional, rather than interstitial, sites in both Si and Ge. Here, compensated doping, where donor-type co-dopants (P or As) compensate the acceptor-type Mn doping, is most effective [45, 46]. By stabilizing Mn in the substitutional sites, they suggest that magnetic ordering is more likely with enhanced Curie temperatures. In addition, the authors also suggest that the variety of behaviors observed for Mn-doped Si and Ge (see below) originate from several factors, including clustering of Mn dopants, second-phase nucleation, and unintentional co-doping (the most likely suspect being oxygen donors). This emphasis to produce Mn in substitutional sites can be contrasted with another approach which instead suggests that one fourth δ-doped Mn layers in Si, where the Mn sites are found to be interstitial, result in half metallic behavior. The authors of this investigation suggested that the interstitial δ-doped layers are more stable than substitutional ones, yet unlike the previous calculations, they predict a magnetic ground state for the *interstitial* Mn layers.

There is at least one recent experimental investigation exploring these ideas by claiming to produce substitutional Mn in co-sputtered $Si_{1-x}Mn_x$ films [47]. Here, X-ray diffraction and absorption methods were employed to demonstrate that Mn substitutes for silicon in the crystal structure [47]. This experiment appears to agree with the theoretical work discussed above by demonstrating that the sites occupied by the Mn dopants in Si are sensitive to the growth and annealing conditions. It is unfortunate that no magnetization data is presented to characterize the magnetic properties of these films so that no comparisons to the predictions of the magnetic properties could be made.

Transition Metal Doping of Silicon Nanowires

The investigation of transition metal doping of silicon nanowires to produce magnetic semiconductors has a similar flavor to that presented above for thin films. There are reports of high Curie temperatures in nanowires that were doped via Mn ion implantation to produce wires with ~1.35 % Mn doping [48]. The saturation magnetization at room temperature was shown to increase with Mn flux and with annealing temperature below 800 °C. For samples annealed at 800 °C a dramatically reduced the magnetic signal was found as the Mn dopants precipitated out of the nanowires, similar to the behavior observed in thin films. For samples annealed at these high temperatures, precipitates of Mn_3O_4 were observed on the nanowire surface due to the poor solubility of Mn in Si. A more in-depth investigation of similarly synthesized nanowires found that the magnetic susceptibility displayed several transitions near 45 K, 640 K, and 815 K which were attributed to the formation of Mn_4Si_7 precipitates, the presence of unintended Fe and Cr impurities, or spinodal decomposition [49].

Although the experimental situation is far from clarified at this time, there are a number of interesting calculations predicting magnetic behavior of silicon nanowires either doped with transition metals or adsorbed on to their surfaces [50–53]. There is also computational work exploring the possibility of magnetism in silicon nanotubes or fullerene structures where transition or rare earth metal atoms are encapsulated [54, 55].

Transition Metal Doping of Crystalline Germanium

A very similar situation exists for Mn doping in Ge where, again, very low solubility of Mn in Ge [43] leads to phase segregation and host of contradictory experimental results. This is not terribly surprising given that there are no Ge-rich phases known to form in the MnGe binary phase diagram [56]. In fact, the highest germanium-rich binary phase known, MnGe (B20 structure), only grows under conditions of high pressure [57], so that it is clearly energetically favorable for Mn-rich clusters and precipitates to nucleate. Initially, there was a great deal of optimism for Mn-doped Ge. For example, in 2002, Park et al. used MBE techniques to grow films of $Ge_{1-x}Mn_x$ while holding the substrate at a cool 70 °C. These films showed some Mn clustering, with nanoscopic regions having a maximum of 10–15 % Mn concentration and a Curie temperature that increased with x from 25 K at $x = 0.005$ to 116 K for $x = 0.035$ [58]. When these films were annealed at temperatures above 300 °C, $Mn_{11}Ge_8$ nanocrystalline precipitates were observed.

Subsequently, there were several reports of ferromagnetism in bulk crystals of $Ge_{1-x}Mn_x$ which displayed ferromagnetic magnetization curves above 300 K [59]. However, these measurements produced temperature-dependent susceptibility curves that had distinct resemblance to those of $Mn_{11}Ge_8$ [60], MnGe [61], or Mn_5Ge_3 [62], leading to the suspicion that the crystals were phase segregated and contained regions where these phases had nucleated. This suspicion was confirmed

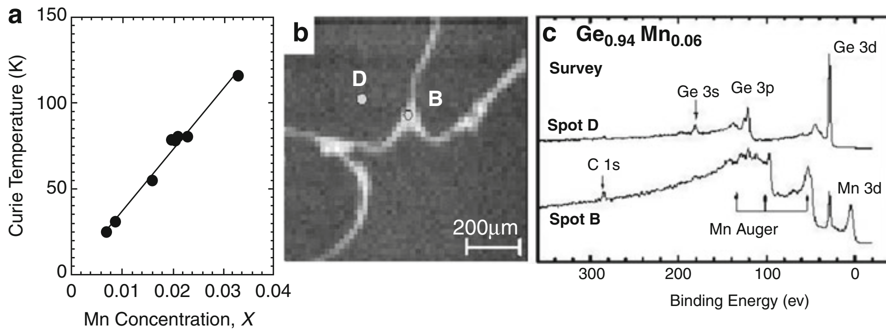

Fig. 4 Mn-doped Ge (**a**) Curie temperature as a function of Mn concentration. (**b**) Scanning electron microscopy image of single crystals of $Ge_{0.94}Mn_{0.06}$. (**c**) Survey spectra from two regions of the crystal-labeled B and D in frame (**a**) demonstrating the germanium-rich regions (D) and Mn-rich regions (B) (Reprinted figures with permission from Kang et al. [62]. Copyright (2005) by the American Physical Society)

by measurements (scanning photoelectron spectroscopy, x-ray absorption spectroscopy, and photoemission spectroscopy) which revealed striped-shaped microstructures where these magnetic second phases segregated from the bulk Ge [63] (see Fig. 4b, c).

More systematic work on thin films followed including carefully controlled MBE growth with very low substrate temperatures (70 °C). This technique produced films without the formation and segregation of MnGe compounds (see Fig. 5) [64]. However, the Mn was still found to cluster, leaving an inhomogeneously doped film. Typical results displayed two Curie temperatures for these films, at 12 and 112 K for $x = 0.05$, where the upper transition was thought to be due to the ordering within Mn clusters that would eventually order globally when cooled to 12 K. Similar results were reported for low-temperature MBE 5 % Mn in Ge films where nanoclustering of the Mn was found along with superparamagnetism below 160 K and spin glass behavior at temperatures less than 15 K [65]. This description is similar to that known as Griffiths phase phenomena as was discovered in the magnetic behavior of Co-doped FeS_2 [66, 67].

It appears that a consensus is forming in which the higher Curie temperatures reported in the early investigations have been mostly ascribed to the formation of Mn_5Ge_3 precipitates, although $Mn_{11}Ge_8$ or even MnGe precipitates are also suspected [68]. In contrast, materials where the substrate temperature was kept below about 100 °C do not display the second-phase precipitates; however, Mn clustering is observed along with lower Curie temperatures. Understanding of these issues is necessary for progress in Mn-doped Ge as a possible magnetic semiconductor. Co-doping of Ge with Mn and Co may be one solution to the clustering and phase segregation as it appears to suppress the nucleation of secondary phases while enhancing the magnetism. Tsui et al. showed that $Co_{ax}Mn_{bx}Ge_{1-x}$ films formed by MBE methods on substrates held at 250 °C and annealed at 450 °C resulted in films with similar high- and low-temperature transitions. Curie temperatures

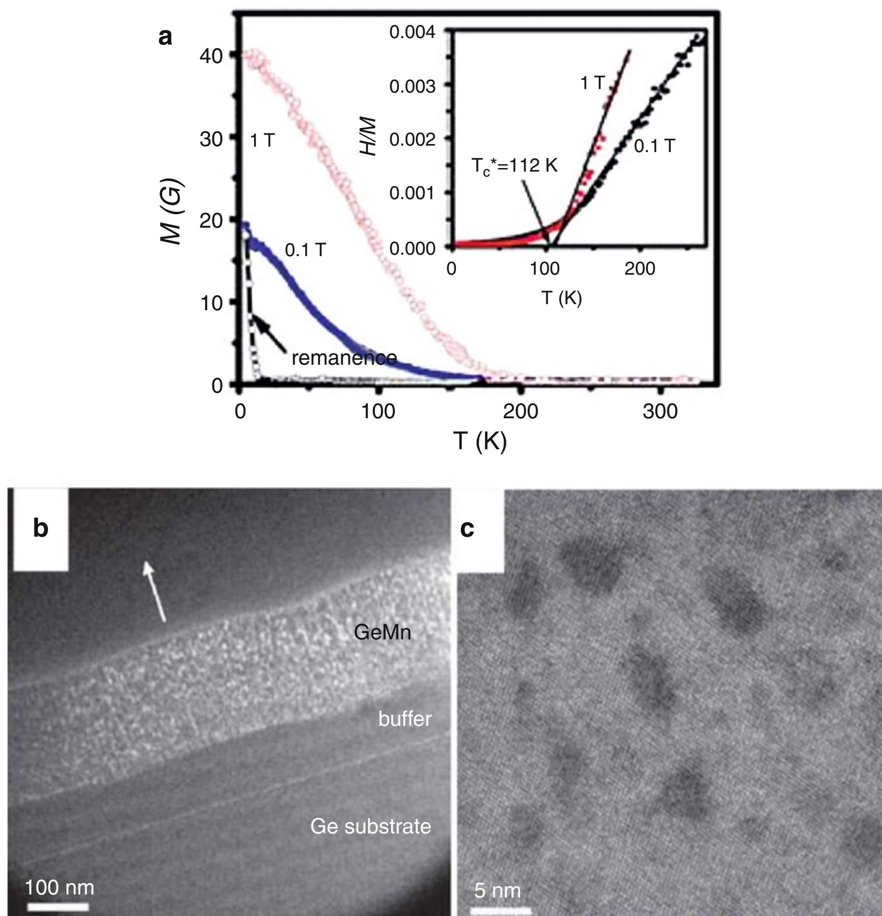

Fig. 5 Molecular beam epitaxy growth of $Ge_{1-x}Mn_x$. (**a**) Magnetization at three fields for an $x = 0.05$ sample grown at a substrate temperature of 70 °C. Inset: inverse magnetic susceptibility of the same sample displaying Weiss temperature above 100 K (Reprinted figure with permission from Li et al. [63]. Copyright (2005) by the American Physical Society). (**b**) Dark field TEM overview of an $x = 0.05$ sample grown with a substrate temperature of 60 °C. *Bright spots* representing 4 nm clusters of increased Mn content can be seen. (**c**) High-resolution TEM micrograph of an $x = 0.05$ sample with the same growth conditions displaying regions of increased Mn concentration on substitutional sites that are coherently bound to the surrounding Ge film (Reprinted figures (**b**, **c**) with permission from Bougeard et al. [64]. Copyright (2006) by the American Physical Society)

corresponding to the higher temperature transition were reported to be as high as 270 K. They found no sign of second phases in electron diffraction, XRD, or TEM measurements [69]. More recently they have followed up on these ideas by performing a systematic investigation of Co co-dopants using very similar synthesis techniques [70]. The conclusion is that the addition of Co enhances the dopant stability and the magnetic behavior of the films.

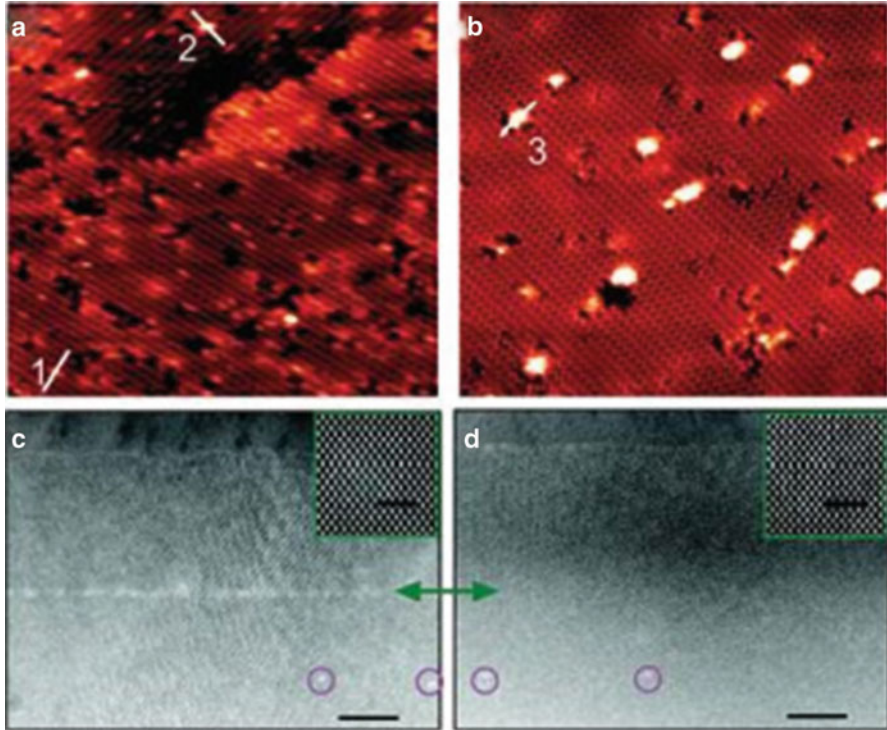

Fig. 6 Subsurfactant epitaxy of Mn in Ge. (**a**, **b**) STM images of 0.05 monolayer of Mn deposited on a germanium (100) surface deposited at 150 K and room temperature respectively. Image sizes are 35 × 32 nm. These were subsequently covered by a germanium epilayer as seen in the STEM images in (**c**) for room temperature growth and (**d**) for 150 K growth. The *green* double pointed *arrow* in (**c**, **d**) indicates the interface between the Ge buffer layer and the epilayer. *Scale bars* in (**c**, **d**) are 20 nm (Reprinted figure with permission from Zeng et al. [70]. Copyright (2008) by the American Physical Society)

One recent publication gives hope for a second possible solution to Mn clustering and second-phase precipitation [71]. Here, Curie temperatures above room temperature were reported in a well-controlled investigation of MBE deposition of small amounts of Mn onto a Ge surface held at 150 K. STM measurements revealed that these Mn atoms were located in the atomic layer just below the Ge surface (see Fig. 6a, b). With subsequent deposition of Ge layers, these Mn atoms were observed to float toward the growth front, resulting in a more homogeneously distributed Mn impurity density (see Fig. 6c, d). What was particularly surprising was that the resulting films showed a ferromagnetic signal in both the magnetization and the Hall effect above room temperature, despite the resulting doping level being 0.25 atomic percent.

Further investigation into the properties of Mn-doped Ge films grown at low temperatures has revealed an interesting phase segregation of Mn-rich and Mn-poor regions for doping levels of a few percent. Jamet et al. report a systematic

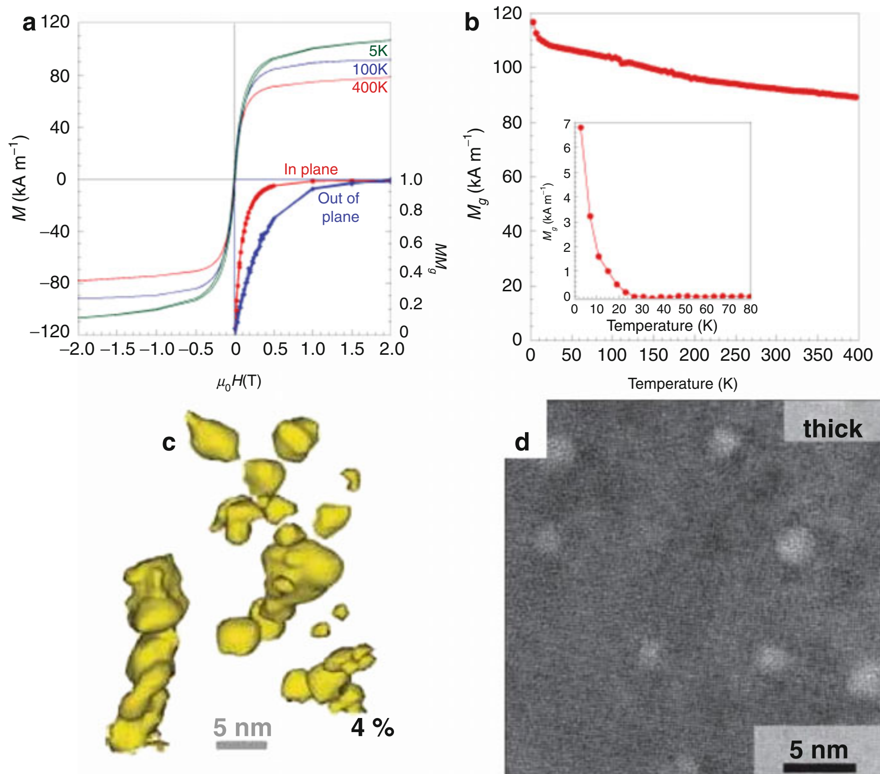

Fig. 7 Phase segregation in co-deposited $Ge_{1-x}Mn_x$ films. (**a**, **b**) Magnetization of clustered Mn-doped Ge films displaying high Curie temperatures (**a**, **b** Reprinted by permission from Macmillan Publishers Ltd [71], Copyright (2006)). (**c**) Pulsed laser atom probe tomography map of Mn-rich clusters in films grown at 60 °C along with (**d**) high-resolution TEM images of a similar sample (**c**, **d** Reprinted with permission from Bougeard et al. [72]. Copyright (2009) American Chemical Society)

investigation of the structure and magnetic properties of co-deposited $Ge_{1-x}Mn_x$ films and found that for substrate temperatures below about 130 °C Mn-rich regions, having a nominal composition of $MnGe_2$, naturally segregate from the Ge matrix into nano-columns of 3 nm diameter and a spacing of 10 nm (see Fig. 7a, b) [72]. These $Ge_{1-x}Mn_x$ regions are thought to have a structure similar to that of the Ge substrate, an elongated diamond structure, with dislocations at the interfaces. Since no $MnGe_2$ equilibrium phase is known to form, and the structure resembled that of Ge, it appeared as though these regions are the long sought after heavily doped semiconductor. In addition, the magnetization measurements displayed Curie temperatures above 400 K with extraordinarily large positive magnetoresistance and an anomalous Hall effect. They also demonstrated that annealing at slightly higher temperatures leads to the nucleation of Mn_5Ge_3 crystallites and a lower Curie temperature. Bougeard et al. confirmed many of these findings but

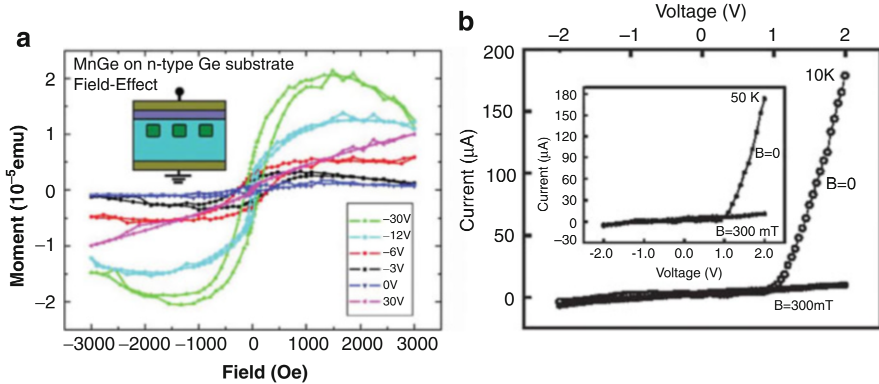

Fig. 8 Demonstration devices fabricated from $Ge_{1-x}Mn_x$ films. (**a**) Gating of a $Ge_{1-x}Mn_x$ film on a *n*-type Ge substrate yields a dramatic change in magnetization. This electric field control of the magnetic properties of thin films may prove useful (Reprinted from Wang et al. [74], Copyright (2008), with permission from Elsevier). (**b**) Germanium-based magnetic diode that acts as a spin valve below the Curie temperature. The structure consists of a $Ge_{1-x}Mn_x$ film deposited on an *n*-type Ge substrate (Reprinted with permission from Majumdar et al. [75]. Copyright (2009), American Institute of Physics)

report that the core of the columns is amorphous and magnetically inactive (see Fig. 7c, d) [73]. This contrasts with the findings of the Grenoble group who report both crystalline nano-columns for the lower temperature growths and amorphous nano-columns for growth temperatures above 150 °C [74]. In addition, Bougeard et al. find that their nano-columns consist of roughly spherical regions strung together "like a string of pearls" rather than in a regular a more regular columnar structure. The conclusion is that the interfaces between the columns and the Ge matrix are important for both the magnetic properties and the transport properties of these systems. All of these papers stress the idea that self-assembled nano-columns could be used as nanowires for the injection of polarized currents. Whether this idea is feasible at a reliable technology remains to be seen.

Despite these difficulties, there have been a few demonstrations of interesting, perhaps useful, phenomena in $Ge_{1-x}Mn_x$ thin films. Wang et al. grew $Ge_{0.96}Mn_{0.04}$ films on Ge substrates via MBE at 70 °C followed by a 400 °C anneal that creates nanoclustered films with no clear sign of either Mn_5Ge_3 or $Mn_{11}Ge_8$ formation in XRD measurements (see Fig. 8a) [75]. These films displayed spin glass-like magnetization curves with a transition temperature well above 300 K and a small-ordered moment (0.4 μ_B/Mn). However, changing the substrate to Si (001) surprisingly increased the ordered magnetic moment to a respectable 1.2 μ_B/Mn. In addition, gating these films via an Al gate over an aluminum oxide dielectric allowed an impressive control over the size of the ordered magnetic moment. The authors claim that the additional holes, provided by the gate electric field, amplify the hole-mediated magnetism of their films, allowing an electric field control over the ferromagnetic properties of their devices. Equally as interesting are the results of Majumdar et al. who have created a diode making use of PLD grown p-type

$Ge_{0.96}Mn_{0.04}$ to form a *pn*-junction with an As-doped Ge film on a Si substrate (Fig. 8b) [76]. They show that at temperatures below the Curie temperature of their film, 50 K, this device acts as an effective spin valve with a sharp turnoff of conduction for forward-biased currents with variation of an applied magnetic field. Further, they claim that the magnetic field creates a Zeeman barrier at the interface creating the effect. It is not clear what role Mn clustering or phase segregation play in these devices as little microscopic characterization was performed in this study.

Thus, there are two main pathways for discovery being pursued: searching for new methods for the production of uniform Mn-doped Ge magnetic semiconductors and the creative use of the natural tendency for segregation of Mn-poor and rich regions which may have very high Curie temperatures. That the inhomogeneous films already demonstrate interesting magnetic properties that can be controlled via electric fields, or visa-versa, lends optimism that Ge-based magnetic semiconductors may have a future as a possible silicon-compatible material for spintronics technologies.

Transition Metal Doping of Amorphous Silicon and Germanium

Because the low solubility of transition metals in group IV semiconductors was recognized as a major hurdle to producing magnetic semiconducting materials that are compatible with silicon, there have been a number of attempts to grow transition metal-doped amorphous Si and Ge. This is an intriguing idea as this approach has the promise to create more homogeneously distributed dopants which may lead to higher Curie temperatures. On the other hand, there are several possible negative aspects to the use of highly disordered materials as magnetic semiconductors, including the likelihood of producing spin glasses instead of ferromagnets and an increased scattering rate for the polarized charge carriers.

The results of the few investigations of Mn-, Cr-, and Fe-doped amorphous Si and Ge have produced somewhat contradictory results, and a clear picture of the cause of the variations observed has not yet evolved. Thus, I present a paraphrasing of the results of a few investigations highlighting the differences and emphasizing the need for continued systematic investigation of the local microscopic structure, dopant homogeneity, and the degree of oxidation of the dopants in these films.

In references [77–79], electron-beam co-evaporation of a transition metal or rare earth elements and Si or Ge produced homogeneously doped amorphous silicon (α-Si) or amorphous Ge (α-Ge) thin films. The growth process of these films included a capping layer to help avoid oxidation of the impurities. These produced interesting low-temperature properties, such as the field-induced insulator-to-metal transition in Gd-doped α-Si [77, 78]. However, only Mn-doped α-Ge yielded a magnetic ground state where a spin glass transition was observed below 10 K [79]. There were distinct differences in the magnetic moment produced when Mn doping α-Si compared to α-Ge. A very small magnetic moment was found in the Si case (0.1 μ_B/Mn), while a much larger one was apparent in the Ge samples

(3 μ_B/Mn). The authors explain these differences based upon the local structure, the likely coordination of the Mn ions with the surrounding group IV elements, and the carrier type (n-type for α-Si and *p*-type for α-Ge).

These experiments stand in stark contrast to several more recent results for transition metals in amorphous Si or Ge fabricated by ion implantation or sputtering that show much higher transition temperatures. For example, Soo et al. [80] used magnetron sputtering techniques to produce highly disordered Mn- and Cr-doped silicon thin films on glass substrates held at room temperature. These films were sputtered using a 20 % H_2 in Ar as a sputtering gas in order to hydrogenate the films, thus reducing the dangling bonds in the amorphous semiconductor. The result was magnetization curves displaying hysteresis to 250 K for Mn and above 300 K for the Cr doping. The size of the ordered magnetic moment was not reported, and no comparison of field-cooled (FC) and zero-field-cooled (ZFC) magnetic susceptibilities was reported, leaving a few questions about the magnetic state of this system. X-ray absorption fine structure spectroscopy measurements were performed on these films which demonstrated no MnSi or CrSi intermetallic phase formation in their films. In addition, these measurements revealed a five- to sixfold coordination of the transition metal ions with Si.

Similar results for co-sputtering of Fe and Ge to form 30–50 % Fe-doped α-Ge films on glass substrates were produced by Qin et al. [81]. Here the substrates were kept at 20 °C and X-ray diffraction and TEM showed no sign of crystalline structures. These disordered metallic films displayed hysteretic magnetization curves at temperatures exceeding 300 K with a saturated magnetic moment of a respectable 1.7 μ_B/Fe. The temperature-dependent susceptibility revealed a FC-ZFC separation near 330 K, suggesting a disordered ferromagnetism or spin glass-like state. Hall effect and ferromagnetic resonance measurements confirmed the magnetic behavior and suggested a uniform magnetic state.

Amorphous germanium thin films can also be produced with heavy Mn ion implantation. Ottaviano et al. [82] found that a 155 nm thick completely amorphized Ge layer was created at the surface of Ge (001) wafers held at 77 K during implantation. X-ray absorption spectroscopy revealed the absence of MnGe phase precipitation, the lack of Mn dimers for Mn concentrations of 4 % or less, and demonstrated that the material was amorphous with Mn substitutions with fourfold coordination rather than interstitials. SQUID measurements showed hysteretic behavior at room temperature with little difference between the FC and ZFC magnetic susceptibility. Interestingly, the magnetic moment measured was very small compared to the sputtered films; only 0.08 μ_B/Mn was apparent in the magnetization measurements, meaning that most of the Mn did not contribute to the ordered magnetic state.

The broad variation of results found in these studies leaves many questions. Why, for example, do the electron-beam evaporated films show a large Mn-related magnetic moment and a low-ordering temperature while the ion-implanted films display a much smaller magnetic moment and a high-ordering temperature? In addition, the question of how the amorphous $Ge_{1-x}Mn_x$ films compare to the Mn-rich clusters in MBE-grown crystalline Ge should be answered. Finally, it is

not clear that these disordered materials can produce highly spin-polarized currents that are necessary for use in technologies. The large scattering rates for charge carriers and spin glass or disordered ferromagnetic states may degrade any useful polarization of currents. Still, this remains an interesting avenue for research as intriguing results, but an incomplete picture, leave plenty of room for discovery.

Magnetic Silicides and Germanides

The review of efforts to create magnetic semiconductors by doping silicon or germanium with transition metals in the previous sections presents a field where there is some progress and where there are certainly avenues for exploration that may lead to discovery. However, the search for magnetic semiconductors that are compatible with silicon is far broader as there are a number of directions for investigation into magnetic and/or semiconducting materials that may be productive. The existence of both magnetic and semiconducting phases among the binary transition metal silicides and germanides makes these materials interesting candidates for the injection of spin currents in silicon. The attractiveness of silicides is clearly a reflection of the fact that many are already in use in the semiconductor industry. In addition, several are known to readily form epitaxially on silicon substrates, leading to expectations that interfacial scattering between silicides and silicon may be minimized. Thus, these materials may be useful to consider for spintronics.

A review of the binary and quasi-binary silicide and germanide materials reveals that there are a number of transition metal, Rare Earth, and actinide compounds that are magnetic. These materials generally fall into three main stoichiometries and crystal structures, although there are several that fall outside of this description.

The first is the Heusler-type, or body-centered cubic, Tm_3Si series with Tm = Fe or Mn and where the Mn compound is antiferromagnetic (AFM) (Neel temperature, $T_N = 23$K) and the Fe compound is ferromagnetic (FM) ($T_C = 808$ K) [83]. There are also variations of these materials with different transition metal substitutions at the various Tm sites of these silicide Heusler-structured materials. Cobalt substitution for Fe or Mn produces ferromagnets with large carrier polarizations such as in Co_2MnSi ($T_C = 985$ K) and Co_2FeSi ($T_C = 1{,}100$ K) [83, 84]. The germanide Fe_3Ge also forms in this crystal structure and is FM having T_C of 638 K, while Mn_3Ge instead forms in either a hexagonal crystal structure with an AFM ordering temperature of $T_N = 395$ K [83, 85] or, with high pressure synthesis, in the Cu_3Au structure with a FM ordering at 400 K [86]. However, $FeMn_2Ge$ ($T_C = 233$ K) and Fe_2MnGe ($T_C = 433$ K) both form in the Heusler structure type and are ferromagnetic as are Co_2MnGe ($T_C = 905$ K) and Rh_2MnGe ($T_C = 450$ K) [83]. There are several investigations of these types of materials grown on silicon and germanium substrates to assess their compatibility with silicon technology [87–91]. A few of these materials, Co_2MnSi, Co_2FeSi [92], and Co_2MnGe, are predicted to be half metallic with high Curie Temperatures and are well lattice matched to GaAs [93, 94]. However, these materials have carrier densities typical of good metals and thus

present the same Schottky barrier issues as other metallic ferromagnets. The reader is referred to the discussion of magnetic alloys having the Heusler structure type in section Magnetic Heusler alloys of this handbook.

These materials have already proven useful as sources of polarized currents for injection into silicon by tunneling through the resulting Schottky barrier [95]. Here an epitaxial Fe_3Si film was grown by low-temperature MBE techniques on a Si (111) substrate with a heavily doped n^+-Si layer near the abrupt silicon-Heusler alloy interface [87]. Evidence for spin accumulation in the Si layer was observed by nonlocal voltage measurements. In addition, epitaxial layers of $Fe_{3-x}Mn_xSi$ have been grown on Ge substrates that display Curie temperatures that exceed room temperature for $x \sim 0.6$ [89]. Band structure calculations of this alloy indicate that for $0.75 < x < 1.5$ half metallicity is expected; however, a lower Curie temperature is found in this range of x.

A second family of silicide compounds that display interesting magnetism is the hexagonal $Fe_xMn_{5-x}Si_3$ compounds which have the Nowotny phase, or $D8_8$, structure. These are FM for $x \geq 3.5$, FM with a transition to helimagnetic, HM, below 60 K for $x = 3.5$, and AFM for $0 \leq x \leq 3.0$ with transition temperatures that rises from 100 to 381 K with x [83, 96]. Mn_5Ge_3 also forms in the $D8_8$ crystal structure, displays ferromagnetism below 295 K [83], and can form epitaxially registered films on Ge (111) surfaces [97]. Fe_5Ge_3 takes on a slightly different hexagonal lattice structure, the $B8_2$ type, and is FM below 485 K [83, 98]. The series $Fe_{5-y}Mn_yGe_3$ can be stabilized for $y \leq 2$ with the Curie temperature decreasing linearly with y down to 326 K [98].

The transition metal monosilicides and germanides form the third family of compounds that display magnetic ground states. These alloys tend to form in a simple cubic structure, B20 (or $P2_13$), which lacks inversion symmetry. The resulting spin-orbit interaction causes a long wavelength twist (wavelengths of between 3 and 70 nm have been reported) of the magnetic moments, helimagnetism, which is often described in terms of the Dzyaloshinskii-Moriya interaction. Small magnetic fields tend to collapse the spirals into a FM state. This grouping includes helimagnets (HM) MnSi ($T_C = 30$ K), $Fe_{1-x}Co_xSi$ ($0 < T_C < 65$ K), the B20 form of FeGe ($T_C = 285$ K), and MnGe which can be synthesized only at high pressure ($T_C = 170$ K) [83, 99–105].

Other FM silicides include $Cr_9Pd_{71}Si_{20}$ ($T_C = 60$ K) [83] and the rare earth compounds Er_5Si_4 ($T_C = 25$ K), Gd_5Si_4 ($T_C = 336$ K), Ho_5Si_4 ($T_C = 76$ K), and Tb_5Si_4 ($T_C = 225$ K), as well as USi ($T_C = 120$ K) [83]. There are also several AFM rare earth silicides such as $GdSi_2$ ($T_N = 27$ K), $HoSi_2$ ($T_N = 18$ K), TbSi ($T_N = 57$ K), and $TbSi_2$ ($T_N = 17$ K) [83]. FM germanides that do not fall into the above categories include Mn_3Ge_2 ($T_C = 283$ K), Mn_2Ge_2Cu ($T_C = 612$ K), $Cr_{11}Ge_{19}$ ($T_C = 98$ K) [106], Fe_2Ge ($T_C = 470$ K), and FeMnGe ($T_C = 245$ K). Antiferromagnetic transition metal germanides include FeGe ($T_N = 412$ K), $FeGe_2$ ($T_N = 190$ K), and $Mn_{3.25}Ge$ ($T_N = 139$ K) [83]. There are a small number of FM rare earth and actinide germanides such as PrGe ($T_C = 39$ K), $PrGe_2$ ($T_C = 19$ K),

UGe_2 (T_C = 52 K) and $PuGe_2$ (T_C = 34.2 K) [83]. Finally there is a long list of AFM rare earth and actinide germanide compounds that include the monogermanides of Sm (T_N = 40 K), Gd (T_N = 62 K), Tb (T_N = 42 K), Dy (T_N = 36 K), Ho (T_N = 18 K), and Er (T_N = 7 K), $REGe_{1.67}$ with RE = Gd (T_N = 450 K) and Dy (T_N = 12 K); the digermanides of Gd (T_N = 450 K), Tb (T_N = 42 K), Dy (T_N = 28 K), and Ho (T_N = 11 K); Re_5Ge_3 compounds of Pr (T_N = 12 K), Gd (T_N = 48 K), Tb (T_N = 85 K), Dy (T_N = 40 K), Ho (T_N = 10 K), and Er (T_N = 31 K); and RE_5Ge_4 compounds Gd (T_N = 15 K), Tb (T_N = 30 K), Dy (T_N = 40 K), Ho (T_N = 21 K), and Er (T_N = 7 K) [83].

There are some clear trends apparent in these lists. The most obvious is that most of the magnetic states occur when the transition metal concentration is larger than that of the Si or Ge. The exceptions are the monosilicides and monogermanides, the compound $Cr_{11}Ge_{19}$, and the rare earth and actinide disilicides and germanides. For the FM materials, Curie temperatures approaching or exceeding room temperature generally occur in the compounds with higher transition metal content. Exceptions to this trend include the B20 phase of FeGe, Gd_5Si_4, and Mn_3Ge_2.

The second important feature in the search for designing magnetic semiconducting phases is the presence of an isostructural, or closely related, small bandgap-insulating phase. This would allow the ability to tune the carrier density and Fermi energy to match that of the host semiconducting substrate, Si or Ge. However, insulating states most commonly occur in compounds where the Si or Ge content is at least as large as the *TM* content. The insulating silicides, with the bandgap energies in parentheses, include the B20 monosilicides FeSi (0.06 eV), RuSi (0.26 eV), and OsSi (0.34 eV); the disilicides $CrSi_2$ (0.35 eV), β-$FeSi_2$ (1.0 eV), $ReSi_2$ (0.13 eV), $OsSi_2$ (1.4 eV); the Nowotny chimney ladder phases $MnSi_{1.7}$ (0.45 eV), $Mn_{11}Si_{19}$ (0.66 eV), and $Mn_{15}Si_{26}$ (0.7 eV); and the 5d silicides Ru_2Si_3 (0.7 eV), $ReSi_{1.75}$ (0.36 eV), Os_2Si_3 (2.3 eV), and Ir_3Si_5 (1.2 eV) [107–109]. Insulating germanides appear to be more rare, although Ru_2Ge_3 has a bandgap of 0.52 eV [109] and RuGe has a small bandgap measured to be 0.15 eV [108].

When considering materials for use as magnetic semiconductors, the features that are desirable include highly polarizable ferromagnetic states with small carrier densities to reduce any Schottky barriers for polarized current injection into semiconductors. The point of collecting the lists of compounds above is that it may be productive to search for families of compounds with both magnetic and insulating materials having the same crystal structure. It is unusual to find ferromagnetic materials with low carrier densities. However, chemical substitutions between a FM compound and an isostructural insulator may yield a magnetic semiconducting series by design. Since only compounds with the Si or Ge concentration at least as large as the transition metal concentration are semiconducting, and with the rare earth materials not showing insulating behavior, the most productive place to search appears to be the monosilicides and germanides. The review of materials presented here indicates several insulating phases having the B20 crystal structure along with a number of isostructural FM phases.

Monosilicides and Monogermanides

As discussed above, many of the 3d, 4d, and 5d transition metal silicides form in the same simple cubic structure in space group $P2_13$ also known as B20 [99]. The electronic structure of these materials varies from simple metallic and paramagnetic, such as in CrSi and CoSi, to insulating with a small bandgap, as in FeSi, RuSi, and OsSi, to helimagnetic, as is well known to occur in MnSi and in $Fe_{1-x}Co_xSi$ [99–105]. Because these materials all form with the same equilibrium crystal structure, chemical substitution at the transition metal site is easily accomplished. In addition, these materials display little proclivity toward the formation of second phases.

The occurrence of magnetic and semiconducting phases, along with the flexibility offered by the wide range of substitutions available, led Manyala et al. to suggest that these materials ought to be considered for spintronics applications [5]. They demonstrated that significant control over the magnetic and electronic properties can be achieved in these materials through chemical substitutions in insulating FeSi [25, 100–103] (see Fig. 9). Either hole, Mn or Al, or electron, Co, doping yields insulator-to-metal transitions with unique properties. Substitutions at the transition metal site leads to the formation of magnetic states; for Mn doping, $Fe_{1-x}Mn_xSi$, a helimagnetic state forms for $x > 0.8$, while for Co doping, $Fe_{1-y}Co_ySi$, helimagnetism is apparent between $0.05 < y < 0.8$ [101]. These magnetic semiconductors display many interesting properties, particularly in their magnetoresistance and Hall effect [25, 100, 101, 110–112].

The monoslicides are also well known for their fascinating magnetic properties. MnSi has long been thought of as a prototypical weak itinerant ferromagnet [104, 105, 113]. More recently, MnSi has been of interest because its Curie temperature can be easily suppressed with pressure so that it was thought a quantum critical point could be accessed [114, 115]. However, the sought after quantum criticality is avoided in a most interesting fashion [114, 115]. Unlike the rare earth heavy fermion metals which most often avoid quantum critical points by entering into an unconventional superconducting state, MnSi is thought to enter a state referred to as a partial magnetic order, similar to the state of liquid crystals. There followed several proposals for the magnetic state of the system under pressure at low temperature that suggest unconventional spin textures [116–119]. These speculations inspired a closer investigation of the so-called A phase of MnSi which exists in a small magnetic field range near $T_c = 30$ K. Muhlbauer et al. discovered through careful neutron scattering studies that this phase is most likely comprised of a skyrmion lattice in a chiral magnet [120]. This experiment was soon followed by Lorentz force microscopy images of thin samples of $Fe_{1-x}Co_xSi$ and FeGe (see below), showing real space images revealing these interesting spin textures [121, 122]. Ideas for stimulating the motion of the skyrmion lattice with small currents have also been demonstrated [123].

However, the monosilicides have the important drawback that the Curie temperatures have not exceeded 65 K. Thus, it may be productive to extend the

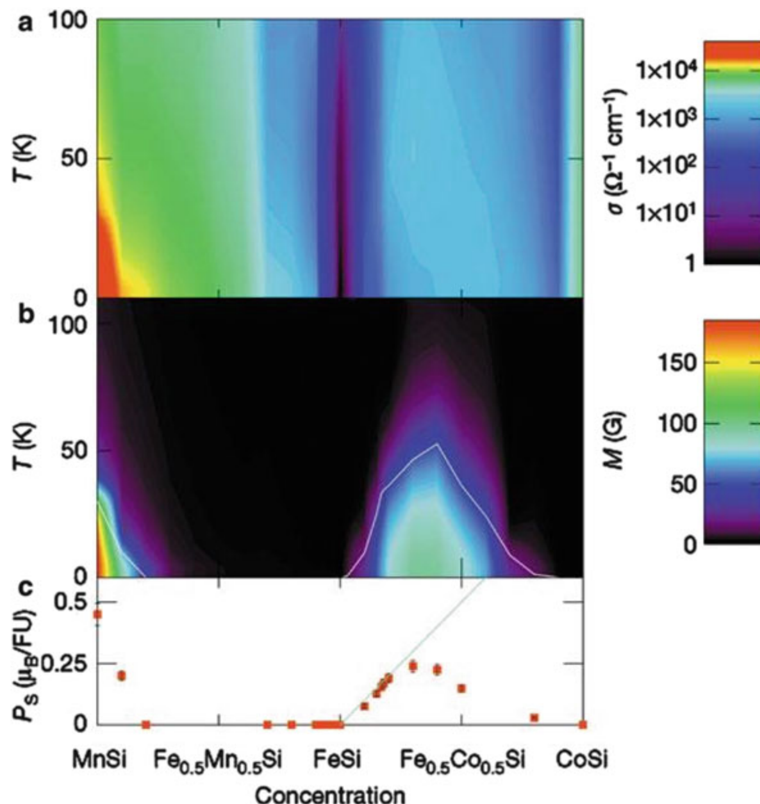

Fig. 9 Transition metal monosilicides having the B20 structure: (**a**) conductivity map (**b**) magnetization at 1 kOe, and (**c**) saturated magnetization as a function of composition from helimagnetic MnSi, through the nonmagnetic insulating phase FeSi, to the diamagetic metal CoSi. *Green line* in (**c**) represents 1 Bohr magneton per Co dopant in FeSi (Reprinted by permission from Macmillan Publishers Ltd: [99], Copyright (2000))

consideration to other isostructural compounds, such as the monogermanides. Although only CrGe forms an equilibrium B20 phase [124], FeGe can be easily grown with in this structure [125], and CoGe and MnGe will form in the B20 lattice under pressure [57, 61]. The important point is that MnGe and FeGe are both helimagnetic metals with elevated Curie temperatures as compared to their silicide equivalents, 285 K for FeGe and 170 K for MnGe [61, 126–128]. These also have interesting transport properties including very large anomalous Hall effects [61, 129]. The monogermanides appear to be compatible with the monosilicides as substitution series, such as $FeSi_{1-x}Ge_x$, are easily synthesized [128]. In this case, there is a first-order transition between the insulating state of the end member FeSi to the HM metallic state of FeGe at x ~ 0.25 [128]. Thus, these materials represent a very flexible Si-based magnetic semiconducting

system that has not been fully explored both in terms of fundamental properties and for suitability for future technologies.

Thin Films of Monosilicides and Monogermanides

The demonstrated ability to grow high-quality thin films and nanostructures of this class of materials is necessary for demonstration experiments and to assess their possible technological relevance. There has been some progress over the past few years toward this goal, and we highlight a few of the reports of successful synthesis.

The growth of silicide films on silicon substrates has a long and successful history. Much effort has been focused on the growth of the transition metal disilicides for metallic interconnects and gates for the microelectronics industry because of the ability to make reliable Ohmic contacts or high-Barrier Schottky contacts as needed. These films were generally found to have a small lattice mismatch with silicon, to be thermally stable, and corrosion resistant [107, 130, 131]. The standard method for silicide formation is to thermally evaporate or sputter the metal onto silicon and then to anneal at temperatures between 200 °C and 600 °C to form the silicide phase [132]. High-quality films with epitaxial registration to the silicon substrates have been achieved for a number of these disilicide phases, as well as several others, by various methods as reviewed in [133]. The most common methods include solid-phase epitaxy (SPE), reactive deposition epitaxy (RDE), and MBE techniques, although ion-beam, or mesotaxy, synthesis has also been demonstrated for some materials [133].

There have also been several successful demonstrations of monosilicide thin film synthesis, revealing an epitaxial registration with silicon substrates. This includes RDE growth of the bulk phase of FeSi with substrate temperatures between 300 °C and 350 °C [134, 135]. MBE growth on Si (111) at room temperature yields epitaxial films of FeSi in the metastable CsCl crystal structure, while annealing at 350 °C transforms these films into polycrystalline films in the bulk (ε-FeSi) structure [136, 137]. Preparation of films using SPE techniques on Si (111) allows the formation of ε-FeSi, CsCl-type FeSi, β-$FeSi_2$, and metastable CaF_2-type $FeSi_2$ phases [138]. The quality of the FeSi and β-$FeSi_2$ phases can be increased by the use of Sb as a surfactant during RDE growth as demonstrated in Ref. [139]. In the same way, high-quality MnSi RDE-synthesized films have been demonstrated with the use of Sb as a surfactant [140, 141]. However, a Sb-Mn-Sb layer is observed at the Si/MnSi interface which acts both as surfactant and as a compliant substrate for stress relief [141], but which may act as a scattering center for the injection of currents from the silicide to the Si. More recently MnSi film growth on Si has been demonstrated using SPE and MBE techniques, and the MBE films were demonstrated to be HM via neutron reflectometry and magnetometry (see Fig. 10). The wave vector for the HM phase was found to be larger than for bulk samples but similar in that it was along the (111) crystal axis in zero applied magnetic field [142, 143].

Using density functional calculations, Hortamani et al. predicted that ultrathin films of MnSi on Si(111) would have large spin polarizations (50 %) at the Fermi level and may be an efficient source of spin-polarized carriers for injection into

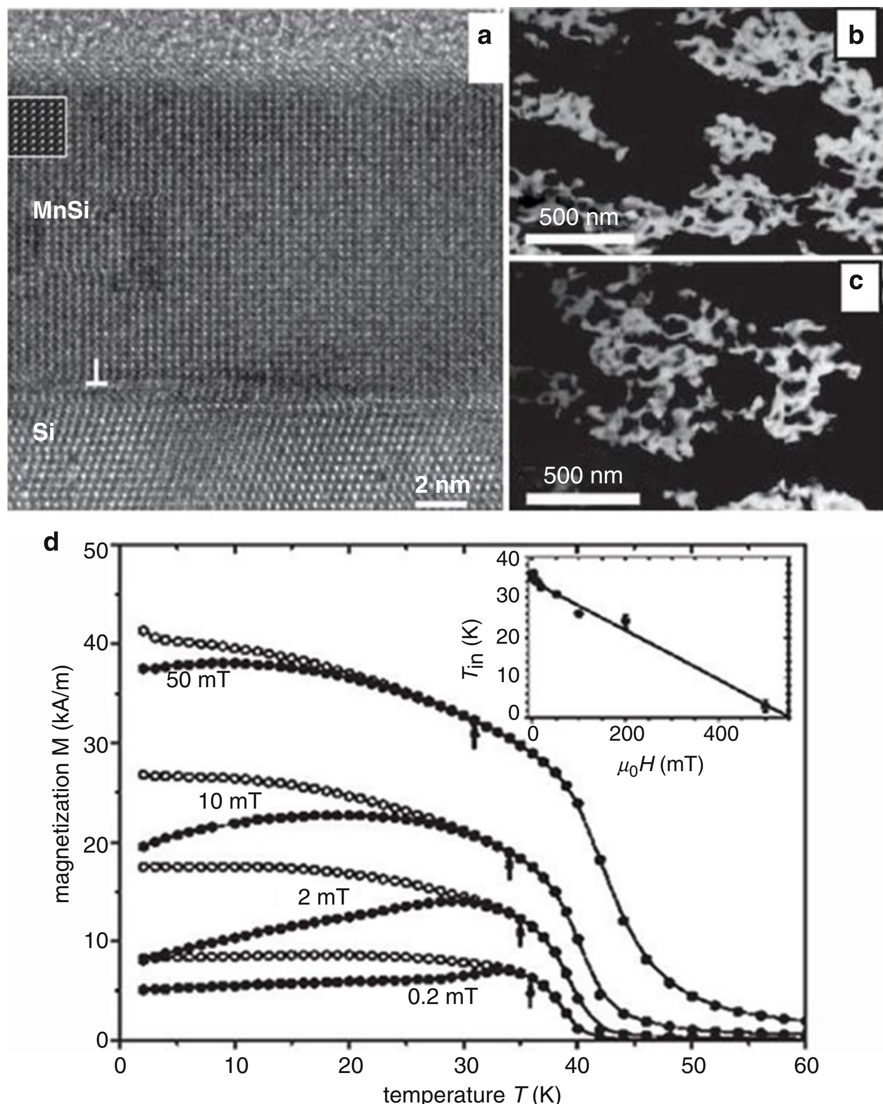

Fig. 10 Epitaxial MnSi thin films. (**a**) High-resolution TEM micrograph of an 11.5 nm thick MnSi thin film grown on a Si (111) substrate via solid-phase epitaxy techniques. The inset displays a HRTEM image simulation. (**b**, **c**) display plane view TEM dark field images of 17.6 nm thick film. Complimentary (0–12) and (−102) reflections were used in (**b**, **c**) which have opposite contrast for the two different crystalline chiralities of the B20 crystal structure and which correspond to the chirality of the helimagnetic state. (**d**) Zero-field-cooled and field-cooled magnetization of an 11.5 nm thick MnSi film showing a substantially higher Curie temperature for these films as compared to bulk samples. The increased Tc is a result of the increased lattice constant due to the substrate induced strain (Reprinted figures (**a–d**) with permission from Karhu et al. [141]. Copyright (2010) by the American Physical Society. Reprinted figures (**b**, **c**) with permission from Karhu et al. [142]. Copyright (2011) by the American Physical Society)

silicon [144, 145]. Motivated by this work, Higashi et al. explored the growth of few monolayer MnSi films grown on Si(111) surfaces produced by the deposition of three monolayers of Mn at room temperature followed by a 250 °C anneal for more than 5 min [146, 147]. They carried out a detailed study of the structure of their films including atomically resolved STM measurements. The results of these in measurements showed that the MnSi (111) plane coincides with the $\left(\sqrt{3} \times \sqrt{3}\right)$ R30° lattice of the Si (111) plane with a 3.2 % mismatch stabilizing the B20 structure so that these films were found to be atomically smooth. The flatness of the surfaces is important because it indicates a very flat interface between the MnSi and the Si so that interface scattering-related reductions of the spin polarization of injected currents may be minimized. In addition, they found that when depositing five monolayers of Mn on the Si substrates, the supply of usable Si at the surface becomes limited causing deep holes and a roughened surface. This conclusion led them to attempt film growth via co-deposition of Mn and Si where they found anomalously flat MnSi films. Magnano et al. have also explored the co-deposition of Mn and Si to create both ultrathin magnetic films (as thin as two monolayers), and surprisingly these films displayed a hint of magnetism appearing at temperatures exceeding room temperature [148, 149]. This additional magnetic signal is thought to be due to Mn atoms with reduced coordination at surfaces or near the film-substrate interface as predicted in [145]. Other investigations of RDE films include [150–152] where thicker films were formed.

A different method for the formation of silicide films, using pulsed laser deposition, PLD, was demonstrated for the B20 $Fe_{1-x}Co_xSi$ system by Manyala et al. [153]. Here, arc-melted $Fe_{1-x}Co_xSi$ targets were employed to grow relatively thick films, 35–500 nm, on Si (111) surfaces held at at 450 °C. The resulting polycrystalline films displayed sharp continuous interfaces with the Si substrates, although there was some evidence for diffusion of Fe into the Si lattice. These films featured smooth surfaces with <0.8 nm root-mean-square surface roughness outside of a small density of droplets common to the PLD growth technique. The magnetic behavior was similar to that of the bulk materials with Curie temperatures between 20 and 30 K; however, the magnetization curves displayed some hysteretic behavior indicative of FM behavior rather than the helimagnetism found in bulk samples.

Monosilicides and Monogermanides Nanostructure Devices

A second route to forming usable structures for spintronics devices is through the synthesis of magnetic metallic and semiconducting nanostructures. Here the challenge is to demonstrate the structural, magnetic, and electronic properties necessary for spin-polarized charge carrier transport in nanowires or nanoparticle systems. Additional challenges lie in the control of the placement and the reliability of electrical contacts to these structures. It is impressive that some of these challenges have been met in a number of interesting nanowire systems, including $Ge_{1-x}Mn_x$ nanowires as reviewed in Ref. [154]. These polycrystalline nanowires grown in anodized alumina oxide membranes can have Curie temperatures above 300 K and

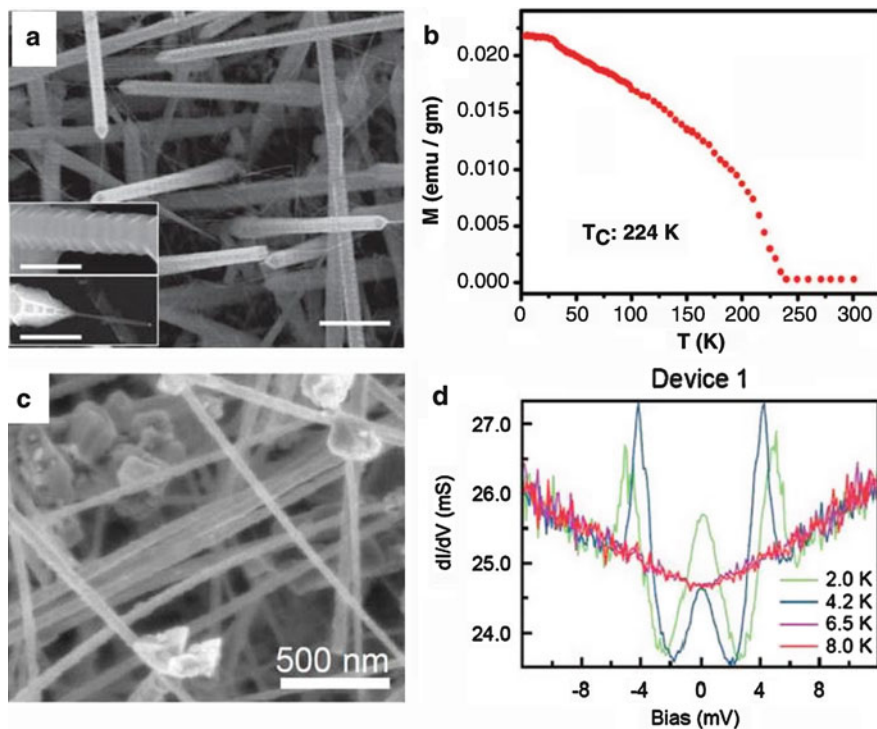

Fig. 11 Nanostructures. (**a**) Field emission scanning electron microscope image of $Ge_{1-x}Cr_x$ nanotowers. Insets show magnified images of *top* and *bottom* of a nanotower. *Scale bars* are 1 μm. (**b**) Magnetization vs. temperature plot for the nanotowers shown in (**a**) (**a**, **b** Reprinted with permission from Katkar et al. [158]. Copyright (2011) American Chemical Society). (**c**) SEM micrograph of $Fe_{1-x}Co_xSi$ nanowires. (**d**) Differential conductance plots from Andreev reflection measurements carried out on the $Fe_{1-x}Co_xSi$ nanowires shown in (**c**) demonstrating the spin polarization of the conduction electrons (**c**, **d** Reprinted (adapted) with permission from DeGrave et al. [173]. Copyright (2011) American Chemical Society)

reasonably high-ordered moments, estimated to be 1.8 μ_B/Mn for $x = 0.01$–0.05. There is no indication of Mn clustering or second-phase formation in these nanowires which can be grown for diameters as small as 35 nm [155, 156]. This same group has followed these impressive findings with an investigation of free-standing crystalline nanowires of $Ge_{1-x}Mn_x$ with x of approximately 0.005–0.1 and diameters between 35 and 180 nm also showing short-ranged magnetism above room temperature. These wires displayed no indication of second-phase formation and a smaller magnetic moment of 0.7 μ_B/Mn [157]. In contrast, nanowires of $Ge_{1-x}Cr_x$ were found to contain Cr-based nanoclusters which were detected along with spin glass-like magnetic phases [158]. However, there is also an interesting report of Cr-doped Ge nanotowers in which only the Ge crystal structure was detected in diffraction measurements, while magnetization measurements indicated ferromagnetism at room temperature [159] (see Fig. 11).

Nanostructures of transition metal silicides are being considered for spintronics applications for the same reasons expressed above for thin film geometries; they offer flexibility since both semiconducting and metallic magnetic ground states can be accessed without the complications of nonequilibrium growth conditions and related tendencies for second-phase nucleation and dopant clustering. A large number of transition metal monosilicide nanowires have been successfully grown including FeSi [160, 161], CoSi [162, 163], $Fe_{1-x}Co_xSi$ [164, 165], MnSi [166, 167], NiSi, PtSi [168], and TiSi [168]. This list of materials is supplemented by a number of other transition metal silicide phases that have been synthesized in nanowire form including Ni_2Si [169]; $Ni_{31}Si_{12}$, Ni_3Si_2, Ni_3Si, $NiSi_2$, $FeSi_2$, $Fe_5(Si_{1-y}Ge_y)_3$ [170]; $MnSi_{2-x}$, α-Mn_5Si_3, β−Mn_5Si_3, β−Mn_3Si [171]; $CrSi_2$ [172, 173]; $TaSi_2$ [168]; and Ti_5Si_3 [168].

I concentrate first on the B20 monosilicide nanowire systems as great progress has been demonstrated over the past few years on the synthesis aspects as well as the characterization of these fascinating structures. The research group of S. Jin at the University of Wisconsin has developed a chemical vapor deposition (CVD) method for the synthesis of free-standing single crystalline nanowires by employing single-source organometallic precursors for the delivery of both the transition metal and the silicon. Precursors such as $M(SiCl_3)_x(CO)_y$, where M is Fe or Co, yield MSix (NW) + yCO(g) + $3x/2$ Cl_2(g) at the surface of an oxide coated silicon wafer held at 750 °C to form the nanowires [160, 162, 164]. This synthesis method does not employ an intentional catalyst and no unintentional catalysts have been discovered. The resulting nanowires are long – more than 10 μm in length and 30–60 nm in diameter which grow along the crystalline (110) direction. By mixing the Co and Fe precursors, or by using *trans*-$Fe(SiCl_3)_2(CO)$ and $CoCl_2$, $Fe_{1-x}Co_xSi$ nanowires with a uniform Co distribution can be grown [164, 174]. The resistivity and magnetoresistance of these nanowires closely resemble that of the bulk materials [164]. In addition, these nanowires display magnetism in the same temperature range as the bulk materials and even display a reasonable spin carrier polarization, ~28 %, as determined by Andreev reflection spectroscopy [174] (see Fig. 11). Similar results have been demonstrated using FeI_2 and CoI_2 as the transition metal precursors [165].

MnSi nanowires can also be grown using similar synthesis techniques; using $MnCl_2$ on Si substrate (SiO_x) produces nanowires 50–400 nm in diameter and as long as 100 μm [166, 167]. The resistivity of these wires can be small (~50 μΩcm in Ref. [69], 500 μΩcm in Ref. [76] at 4 K) with temperature and magnetic field dependencies very much like bulk materials, suggesting that there is helimagnetic transition above 30 K. Seo et al. show that MnSi nanowires grown in this manner display magnetic susceptibility and magnetization that closely resemble that of the bulk material [167]. A second method for forming single crystal MnSi nanowires was demonstrated by Lin et al. [20] using a solid-state reaction of Mn with Si nanowires. This method created atomically sharp interfaces between the MnSi and Si nanowires, allowing an exploration of polarized spin currents through the Si section of the nanowire via the magneto-transport. They were thus able to demonstrate spin-polarized current injection and detection in a silicide/silicon nanowire system.

Recently, FeSi nanowires with Fe_3O_4 nanoheads were created via a simple CVD technique making use of gold as a catalyst [161]. Here gold-coated Si (100) surfaces were placed inside a tube furnace held at 1,100 °C and exposed to Fe_2O_3 vapor carried by a mixture of Ar and H_2 gas. FeSi nanowires with a rather narrow distribution of diameters of ~30 nm were found to grow with a similar diameter capping of Fe_3O_4 nanoparticles. The authors point out that these unique structures would be ideal as sensors for magnetic force microscopy (MFM) applications.

The progress outlined here has led to much optimism for spintronics devices based upon silicide nanowire structures. One important aspect of silicide nanowires in this context is the availability of both ferromagnetic and semiconducting materials. In the monosilicides systems, FeSi is known to be a small gap semiconductor which can be made metallic and magnetic when doped with Co. $CrSi_2$ is also semiconducting and single crystal nanowires of this material grown by CVD methods have been shown to behave as degenerate semiconductors [172, 173]. In addition, the spatial confinement and subtle structural differences of nanostructured materials as compared to bulk materials may result in behavioral differences. This is apparent, for example, in nanowires of CoSi and FeSi, which are diamagnetic or paramagnetic in bulk samples and have been reported to be ferromagnetic at room temperature [163, 175]. CoSi nanowires of diameter between 20 and 60 nm and lengths of tens of microns were grown by Seo et al., employing a technique that relies on a metal halide carrier to transport the metal to a heated Si substrate. Diffraction experiments revealed the B20 structure with several extra diffraction peaks indicating that there was a superlattice structure, while magnetometry measurements revealed FM behavior to at least room temperature. This is to be contrasted by CoSi grown by an organometallic single-source precursor [162] which revealed no superstructure diffraction peaks. Similarly, Hung et al. synthesized FeSi nanowires via CVD techniques that differed from previous investigations by growing along a (10-1) crystal axis. These nanowires had high room temperature resistivity (2.6 mΩcm) and ferromagnetic magnetizations at 300 K. This can be compared to the FeSi nanowires grown by single-source precursor methods where the growth axis is along the (110) crystal axis and where transport measurements reveal a much smaller resistivity of 210 μΩcm [160]. Another example of the differences that can occur between bulk and nanostructured materials has been observed in arrays $Si/Mn_{27}Si_{47}$ core/shell nanowires synthesized by reacting Si nanowires with $MnCl_2$ at elevated temperatures [176]. These wires exhibited ferromagnetism with a Curie temperature of 150 K, much higher than that of bulk samples of $MnSi_{1.7}$.

While the variation in physical properties observed indicates that nanostructured silicides may be a rich area for investigation, careful characterization will be needed to understand and control the properties of these nanostructures if these differences are to be exploited in device technologies. It is clear that systematic investigation continues to produce interesting discoveries in this field [170].

There has not nearly as much reported about germanide nanowires; however, there is one intriguing result that I draw your attention to. The growth of monoclinic FeGe on a Ge substrate was demonstrated by Zeng et al. where they show that the

presence of the substrate tends to compress the lattice constants as compared to the bulk material. Whereas monoclinic FeGe is antiferromagnetic, the compression leads to strongly ferromagnetic behavior with transition temperatures near 200 K [177]. There is also a publication describing the synthesis, structural, and electrical properties of NiGe nanowires and ε-Ni_5Ge_3 nanowires that can be formed by thermal annealing of the NiGe wires [178]. These wires were highly metallic; however, there is no report on the magnetic properties of these structures. Because transition metal germanide phases often display Curie temperatures nearing and exceeding room temperature, the investigation of nanostructures of these phases appears to be an avenue for exploration where few experiments have been performed.

Dilute SiC-Based Magnetic Semiconductors

Silicon carbide is a wide bandgap material, 3.3 eV, that occurs in a large number of polytypes and which has many interesting and useful properties. There have been several attempts to produce magnetic semiconducting behavior in SiC materials via doping of transition metal elements. Early work included ion implantation of Fe, Ni, or Mn into bulk Al-doped 6H-SiC by Theodoropoulou et al. which yielded regions of doping levels near 3–5 atomic % [179]. They found no evidence of second-phase formation in their samples with magnetization measurements yielding FM transitions at 50 K for Ni doping, 250 K for Mn, and 270 K for Fe doping. The origin of the magnetism in their samples was not clear, and the authors point out that further experiments are needed to identify the origin of the magnetism [179]. Later work on Fe-doped 6H-SiC by Stromberg et al. [180] using Fe ion implantation, and Song et al. [181] using polycrystalline powders, identified the formation of Fe_3Si precipitates in their samples and suggested that the ferromagnetic magnetization appearing near room temperature was due to this phase.

Polycrystalline bulk samples of SiC doped with Mn also revealed evidence of ferromagnetism near 250 K [182, 183]. However, there is only a small dependence of the Curie temperature on Mn concentration even for Mn concentrations less than 0.1 %. This lack of variation with Mn doping level suggests that the magnetism may be due to the presence of a secondary phase. Unlike the case of Fe doping in SiC, identifying a likely second phase is not straightforward since there are no bulk MnSi ferromagnetic phases with Curie temperatures nearly that high. Song et al. [184] have also demonstrated that Al dopants in polycrystalline samples of SiC stabilizes the 4H polytype and that co-doping of Al and Cr leads to a disordered FM magnetization with a transition at fairly high temperature.

The doping of SiC nanowires with transition metal impurities has also been demonstrated for the case of V by Seong et al. [185]. Part of the motivation for these investigations comes from their electronic structure calculations that indicated the presence of ferromagnetism and half metallic ground states for Mn-, Cr-, and V-doped semiconductors with cubic lattice structures including SiC and AlN. However, the experiments on V-doped SiC nanowires only indicated magnetism

at very low temperature (10 K). Other electronic structure calculations include that by Shaposhnikov and Sobolev [186] who predict half metallic states for Cr and Mn substitutions and a paramagnetic ground state for Fe doping. In addition, Los et al. [187] employed density functional theory ab initio methods to predict ferromagnetism above room temperature in Mn-doped SiC.

Summary and Concluding Remarks

The continuing search for materials that are both magnetic and semiconducting and that are compatible with silicon technology has yielded many interesting results that I have attempted to highlight here. The search for such a difficult-to-achieve combination of properties has included many attempts to effectively substitute transition metal elements into films of Si or Ge in an attempt to make these prototypical semiconductors magnetic. However, the very low solubility of transition metals in group IV elemental semiconductors apparently makes producing a homogeneous system very difficult even when growth temperatures kept low. This difficulty has led many to consider novel and creative methods for synthesizing homogeneously doped semiconductors. A second approach is to use intermetallic compounds such as silicides and germanides to provide a source of polarized electrons, and I have outlined several productive strategies for creating highly ordered thin films and nanowires of these materials.

Despite this large effort and enticing preliminary successes, a convincing demonstration of a materials system that would be truly useful in a technology is still lacking. Many questions about the origin of the measured magnetic response in the doped semiconductors remain as they have not yet been adequately addressed. The significant progress made to date and the interesting discoveries outlined here indicate that this line of research will continue to produce novel materials systems with unusual, and perhaps useful, physical properties in the near future. In addition, because devices that would effectively combine the charge and spin properties of conducting electrons, or that simply make use of spin currents without any accompanying charge transport, have great promise to advance a wide array of technologies, investigation into silicon-based magnetic semiconductors is sure to continue. As a result I expect that new phenomena will also continue to emerge from these efforts.

Directions for Future Research

It is clear from the previous attempts to produce magnetic semiconductors via transition metal doping of silicon and germanium that creative methods are necessary for producing homogeneously doped semiconductors in order to overcome the natural tendency for transition metal clustering and phase segregation. It appears that co-doping, inclusion of a second dopant along with the Mn or Fe expected to produce the magnetism, may be a productive line for future research.

The preliminary experiments that have been performed have shown some promise that co-doping may change the tendencies for clustering or for forming interstitial dopants. In addition, the method of subsurfactant epitaxy demonstrated by Zeng and coworkers [71] represents the type of new ideas that may be necessary to produce nonequilibrium Mn-doped group IV semiconductors. The exquisite control over growth and morphology that modern surface science promises can only add to the optimism that solutions to these issues will be found.

These same techniques are beginning to be employed to explore the growth of magnetic transition metal silicides and germanides. These systems are interesting because of the control offered by substitution series which do not show tendencies for second-phase formation or dopant clustering. However, there are many challenges that remain and that I expect will receive much attention in the coming years. This includes the modification or discovery of materials so that Curie temperatures can be pushed well above room temperature. Other important experiments that demonstrate that polarized currents can be effectively injected into silicon without either substantial interface scattering or having to overcome large Schottky barriers remain to be carried out. The very impressive experiments demonstrating the synthesis of highly ordered epitaxial MnSi thin films with enhanced Curie temperatures due to possibly controllable interfacial strain [142, 143] indicates that this should be a productive future direction for research. Finally, I mention the necessity for the demonstration of polarized current production, as well as the efficient manipulation and effective electrical contact for nanowire devices represents a set of highly promising avenues for discovery. Demonstrating these properties in nanowires and nanotubes will be central to showing that these interesting structures may be useful in future device technologies.

References

1. Cheng JL, Wu MW, Fabian J (2010) Theory of the spin relaxation of conduction electrons in silicon. Phys Rev Lett 104:016601
2. Appelbaum I, Huang BQ, Monsma DJ (2007) Electronic measurement and control of spin transport in silicon. Nature 447:295–298
3. Huang BQ, Monsma DJ, Appelbaum I (2007) Coherent spin transport through a 350 micron thick silicon wafer. Phys Rev Lett 99:177209
4. Huang BQ, Jang H-J, Appelbaum I (2008) Geometric dephasing-limited Hanle effect in long-distance lateral silicon spin transport devices. Appl Phys Lett 93:162508
5. Lepine DJ (1970) Spin resonance of localized and delocalized electrons in phosphorus-doped silicon between 20 and 30 degrees K. Phys Rev B 2:24292439
6. Lancaster G, van Wyk JA, Schneider EE (1964) Spin-lattice relaxation of conduction electrons in silicon. Proc Phys Soc 84:19–24
7. Ochiai Y, Matsuura E (1976) ESR in heavily doped n-type silicon near a metal-nonmetal transition. Phys Status Solidi A 38:243–252
8. Quirt JD, Marko JR (1972) Absolute spin susceptibilities and other ESR parameters of heavily doped n-type silicon. 1. Metallic samples. Phys Rev B 5:1716–1728
9. Pifer JH (1975) Microwave conductivity and conduction-electron spin-resonance linewidth of heavily doped Si:P and Si:As. Phys Rev B 12:4391–4402

10. Kennedy TA, Pifer JH (1975) Electron-paramagnetic-resonance study of metallic Si-P with iron. Phys Rev B 11:2017
11. Ue H, Maekawa S (1971) Electron-spin-resonance studies of heavily phosphorus-doped silicon. Phys Rev B 3:4232–4238
12. Fabian J, Matos-Abiague A, Ertler C, Stano P, Zutic I (2007) Semiconductor spintronics. Acta Phys Slovaca 57:565–907
13. Huang B, Monsma DJ, Appelbaum I (2007) Experimental realization of a silicon spin field-effect transistor. Appl Phys Lett 91:072501
14. Lu Y, Li J, Appelbaum I (2011) Spin-polarized transient electron trapping in phosphorus-doped silicon. Phys Rev Lett 106:217202
15. Lu Y, Appelbaum I (2010) Reverse Schottky-asymmetry spin current detectors. Appl Phys Lett 97:162501
16. Kikkawa JM, Awschalom DD (1998) Resonant spin amplification in n-type GaAs. Phys Rev Lett 80:4313–4316
17. Schmidt G, Ferrand D, Molenkamp W, Filip AT, van Wees BJ (2000) Fundamental obstacle for electrical spin injection from into a diffusive semiconductor. Phys Rev B 62: R4790–R4793
18. Kiziroglou ME (2005) Electrodeposition of Ni-Si Schottky barriers. IEEE Trans Magn 41:2639–2641
19. Maeda Y, Hamaya K, Yamada S, Ando Y, Yamane K, Miyao M (2010) High-quality epitaxial CoFe/Si(111) heterostructures fabricated by low-temperature molecular beam epitaxy. Appl Phys Lett 97:192501
20. Kiziroglou ME, Li X, Zhukov AA, de Groot PAJ, de Groot CH (2008) Thermionic field emission at electrodeposited Ni-Si Schottky barriers. Solid State Electron 52:1032–1038
21. Lin Y-C, Chen Y, Shaios A, Huang Y (2010) Detection of spin polarized carrier in silicon nanowire with single crystal MnSi as magnetic contacts. Nano Lett 10:2281–2287
22. Uhrmann T, Dimopoulos T, Kovacs A, Kohn A, Weyers S, Paschen U, Smoliner J, Bruckl H (2009) Evaluation of Schottky and MgO-based tunnelling diodes with different ferromagnets for spin injection in n-Si. J Phys D Appl Phys 42:145114
23. Min BC, Motohashi K, Lodder C, Jansen R (2006) Tunable spin-tunnel contacts to silicon using low-work-function ferromagnets. Nat Mater 5:817–822
24. Patel RS, Dash SP, de Jong MP, Janson R (2009) Magnetic tunnel contacts to silicon with low-work-function ytterbium nanolayers. J Appl Phys 106:016107
25. Manyala N, Sidis Y, DiTusa JF, Aeppli G, Young DP, Fisk Z (2004) Large anomalous Hall effect in a silicon-based magnetic semiconductor. Nat Mater 3:255–262
26. Zutic I, Fabian J, Erwin SC (2006) Spin injection and detection in silicon. Phys Rev Lett 97:026602
27. Ohno H, Shen A, Matsukura F, Oiwa A, Endo A, Katsumoto S, Iye Y (1996) (Ga, Mn)as: a new diluted magnetic semiconductor based on GaAs. Appl Phys Lett 69:363–365
28. Olejnik K, Owen MHS, Novak V, Masek J, Irvine AC, Wunderlich J, Jungwirth T (2008) Enhanced annealing, high Curie temperature, and low-voltage gating in (Ga, Mn)as: a surface oxide control study. Phys Rev B 78:054403
29. Zhang FM, Zeng Y, Gao J, Liu XC, Wu XS, Du YW (2004) Ferromagnetism in Mn-doped silicon. J Magn Magn Mater 282:216–218
30. Bolduc M, Awo-Affouda C, Stollenwerk A, Huang MB, Ramos FG, Agnello G, LaBella VP (2005) Above room temperature ferromagnetism in Mn-ion implanted Si. Phys Rev B 71:033302
31. Jiang Y, Liu JF, Sun Y, Xu PS, Sun ZH, Pan ZY, Yan WS, Wei SQ (2008) Structural study of Mn_xSi_{1-x} magnetic semiconductor thin films. Acta Phys Sin 57:4322–4327
32. Nakayama H, Ohta H, Kulatov E (2001) Growth and properties of super-doped Si: Mn for spin-photonics. Phys B 302:419–424
33. Bolduc M, Awo-Affouda C, Ramos FG, LaBella VP (2006) Annealing temperature effects on the structure of ferromagnetic Mn-implanted Si. J Vac Sci Technol 24:1648–1651

34. Awo-Affouda C, Bolduc M, Huang MB, Ramos FG, Dunn KA, Theil B, Agnello G, LaBella VP (2006) Observation of crystallite formation in ferromagnetic Mn-implanted Si. J Vac Sci Technol A 24:1644–1647
35. Zhou S, Potzger K, Zhang G, Mucklich A, Eichhorn F, Schnell N, Grotzschel R, Schmidt B, Skorupa W, Helm M, Fassbender J, Geiger D (2007) Structural and magnetic properties of Mn-implanted Si. Phys Rev B 75:085203
36. Bak-Misiuk J, Misiuk A, Romanowski P, Barcz A, Jakiela R, Dynowska E, Domagala JZ, Caliebe W (2009) Stress-mediated redistribution of Mn in annealed Si:Mn. Mater Sci Eng B 159–160:99–102
37. Woodbury HH, Ludwig GW (1960) Spin resonance of transition metals in silicon. Phys Rev 117:102
38. Higgins JM, Schmitt AL, Guzei IA, Jin S (2008) Higher manganese silicide nanowires of nowotny chimney ladder phase. J Am Chem Soc 130:16086
39. Hu J, Kurokawa T, Suemasu T, Takahara S, Itakura M, Tatsuoka H (2009) Growth of manganese silicide layers on Si substrates using MnCl(2) source. Phys Status Solidi A 206:233–237
40. Liu HJ, Owen JHG, Miki K, Renner C (2011) Manganese silicide nanowires on Si(001). J Phys Condens Matter 23:172001
41. Gottlieb U, Sulpice A, Lambert-Andron B, Laborde O (2003) Magnetic properties of single crystalline Mn_4Si_7. J Alloy Comp 361:13–18
42. Men'shov VN, Tugushev VV, Caprara S (2010) Spin-fluctuation mediated high-temperature ferromagnetism in Si:Mn dilute magnetic semiconductors. Eur Phys J B 77:337–343
43. Yabuuchi S, Ono Y, Nagase M, Kageshima H, Fujiwara A, Ohta E (2008) Ferromagnetism of manganese-silicide nanoparticles in silicon. Jpn J Appl Phys 47:4487
44. Zhang ZZ, Partroens B, Chang K, Peeters FM (2008) First-principles study of transition metal impurities in Si. Phys Rev B 77:155201
45. Chen H, Zhu WG, Kaxiras E, Zhang ZY (2009) Optimization of Mn doping in group-IV-based dilute magnetic semiconductors by electronic codopants. Phys Rev B 79:235202
46. Zhu WG, Zhang ZY, Kaxiras E (2008) Dopant-assisted concentration enhancement of substitutional Mn in Si and Ge. Phys Rev Lett 100:027205
47. Ye J, Jiang Y, Liu QH, Yao T, Pan ZY, Oyanagi H, Sun ZH, Yan WS, Wei SQ (2009) Cosputtered Mn-doped Si thin films studied by x-ray spectroscopy. J Appl Phys 106:103517
48. Wu HW, Tsai CJ, Chen LJ (2007) Room temperature ferromagnetism in Mn+-implanted Si nanowires. Appl Phys Lett 90:043121
49. Ko V, Teo KL, Liew T, Chong TC, MacKenzie M, MacLaren I, Chapman JN (2008) Origins of ferromagnetism in transition-metal doped Si. J Appl Phys 104:033912
50. Durgun E, Akman N, Ciraci S (2008) Functionalization of silicon nanowires with transition metal atoms. Phys Rev B 78:195116
51. Giorgi G, Cartoixa X, Sgamellotti A, Rurali R (2008) Mn-doped silicon nanowires: first-principles calculations. Phys Rev B 78:115327
52. Durgun E, Cakir D, Aikman N, Ciraci S (2007) Half-metallic silicon nanowires: first-principles calculations. Phys Rev Lett 99:256806
53. Xu Q, Li JB, Li SS, Xia JB (2008) The formation and electronic structures of 3d transition-metal atoms doped in silicon nanowires. J Appl Phys 104:084307
54. Singh AK, Kumar V, Kawazoe Y (2004) Metal encapsulated nanotubes of silicon and germanium. J Mater Chem 14:555–563
55. Wang J, Liu Y, Liu YC (2010) Magnetic silicon fullerene. Phys Chem Chem Phys 12:11428
56. Massalski TB, Okamoto H, Subramanian PR, Kacprzak L (eds) (1990) Binary phase diagrams, 2nd edn. ASM International, Materials Park, publisher Scott WW Jr
57. Takizawa H, Sato T, Endo T, Shimada M (1988) High-pressure synthesis and electrical and magnetic-properties of MnGe and CoGe with the cubic B20 structure. J Solidi Status Chem 73:40–46

58. Park YD, Hanbicki AT, Erwin SC, Hellberg CS, Sullivan JM, Mattson JE, Ambrose TF, Wilson A, Spanos G, Joniker BT (2002) A group-IV ferromagnetic semiconductor: Mn_xGe_{1-x}. Science 295:651–654
59. Cho S, Choi S, Hong SC, Kim Y, Ketterson JB, Kim B-J, Kim YC, Jung J-H (2002) Ferromagnetism in Mn-doped Ge. Phys Rev B 66:033303
60. Yamada N, Maeda K, Usami Y, Ohoyama T (1986) Magnetic-properties of intermetallic compound $Mn_{11}Ge_8$. J Phys Soc Jpn 55:3721–3724
61. Kanazawa N, Onose Y, Arima T, Okuyama D, Ohoyama K, Wakimoto S, Kakurai K, Ishiwata S, Tokura Y (2011) Large topological Hall effect in a short-period helimagnet MnGe. Phys Rev Lett 106:156603
62. Tawara Y, Sato K (1963) On magnetic anisotropy of single crystal of Mn5Ge3. J Phys Soc Jpn 18:773–777
63. Kang J-S, Kim G, Wi SC, Lee SS, Choi S, Cho S, Han SW, Kim KH, Song HJ, Shin HJ, Sekiyama A, Kasai S, Suga S, Min BI (2005) Spatial chemical inhomogeneity and local electronic structure of Mn-doped Ge ferromagnetic semiconductors. Phys Rev Lett 94:147202
64. Li AP, Wendelken JF, Shen J, Feldman LC, Thompson JR, Weitering HH (2005) Magnetism in Mn_xGe_{1-x} semiconductors mediated by impurity band carriers. Phys Rev B 72:195205
65. Bougeard D, Ahlers S, Trampert A, Sircar N, Abstreiter G (2006) Clustering in a precipitate-free GeMn magnetic semiconductor. Phys Rev Lett 97:237202
66. Guo S, Young DP, Macaluso RT, Browne DA, Henderson NL, Chan JY, Henry LL, DiTusa JF (2010) Magnetic and thermodynamic properties of cobalt-doped iron pyrite: Griffiths phase in a magnetic semiconductor. Phys Rev B 81:144423
67. Guo S, Young DP, Macaluso RT, Browne DA, Henderson NL, Chan JY, Henry LL, DiTusa JF (2008) Discovery of the Griffiths phase in the itinerant magnetic semiconductor $Fe_{1-x}Co_xS_2$. Phys Rev Lett 100:017209
68. Gunnella R, Morresi L, Pinto N, Di Cicco A, Ottaviano L, Passacantando M, Verna AM, Impellizzeri G, Irrera A, d'Acapito F (2010) Localization of the dopant in Ge: Mn diluted magnetic semiconductors by x-ray absorption at the Mn K edge. J Phys Condens Matter 22:216006
69. Tsui F, He L, Ma L, Tkachuk A, Chu YS, Nakjima K, Chikyow T (2003) Novel germanium-based magnetic semiconductors. Phys Rev Lett 91:177203
70. Collins BA, Chu YS, He L, Zhong Y, Tsui F (2008) Dopant stability and strain states in Co and Mn-doped Ge (001) epitaxial films. Phys Rev B 77:193301
71. Zeng C, Zhang ZY, van Benthem K, Chisholm MF, Weitering HH (2008) Optimal doping control of magnetic semiconductors via subsurfactant epitaxy. Phys Rev Lett 100:066101
72. Jamet M, Barski A, Devillers T, Poydenot V, Dujardin R, Bayle-Guillemaud P, Rothman J, Bellet-Amalric E, Marty A, Cibert J, Mattana R, Tatarenko S (2006) High-Curie-temperature ferromagnetism in self-organized $Ge_{1-x}Mn_x$ nanocolumns. Nat Mater 5:653–659
73. Bougeard D, Sircar N, Ahlers S, Lang V, Abstreiter G, Trampert A, LeBeau JM, Stemmer S, Saxey DW, Cerezo A (2009) $Ge_{1-x}Mn_x$ clusters: central structural and magnetic building blocks of nanoscale wire-like self-assembly in a magnetic semiconductor. Nano Lett 9:3743–3748
74. Jain A, Jamet M, Barski A, Devillers T, Porret C, Bayle-Guillemaud P, Gambarelli S, Maurel V, Desfonds G (2010) Investigation of magnetic anisotropy of (Ge, Mn) nanocolumns. Appl Phys Lett 97:202502
75. Wang KL, Zhao Z, Khitun A (2008) Spintronics for nanoelectronics and nanosystems. Thin Solid Films 517:184–190
76. Majumdar S, Das AK, Ray SK (2009) Magnetic semiconducting diode of p-$Ge_{1-x}Mn_x$/n-Ge layers on silicon substrate. Appl Phys Lett 94:122505
77. Bokacheva L, Teizer W, Hellman F, Dynes RC (2004) Variation of the density of states in amorphous GdSi at the metal-insulator transition. Phys Rev B 69:235111

78. Teizer W, Hellman F, Dynes RC (2000) Magnetic field induced insulator to metal transition in amorphous-Gd_xSi_{1-x}. Solid State Commun 114:81
79. Zeng L, Cao JX, Helgren E, Karel J, Arenholz E, Ouyang L, Smith DJ, Wu RQ, Hellman F (2010) Distinct local electronic structure and magnetism for Mn in amorphous Si and Ge. Phys Rev B 82:165202
80. Soo YL, Yao JH, Wang CS, Chang SL, Hsieh CA, Lee JF, Chin TS (2010) Local structures and concentration dependence of magnetic properties in Cr- and Mn-doped amorphous silicon ferromagnetic thin films. Phys Rev B 81:104104
81. Qin Y-F, Yan S-S, Kang S-S, Xiao S-Q, Zhang Q, Yao X-X, Xu T-S, Tian Y-F, Dai Y-Y, Liu G-L, Chen Y-X, Mei L-M, Ji G, Zhang Z (2011) Homogeneous amorphous Fe_xGe_{1-x} magnetic semiconductor films with high Curie temperature and high magnetization. Phys Rev B 83:235214
82. Ottaviano L, Continenza A, Profeta G, Impellizzeri G, Irrera A, Gunnella R, Kazakova O (2011) Room-temperature ferromagnetism in Mn-implanted amorphous Ge. Phys Rev B 83:134426
83. See Bibliography of Magnetic Materials and Tabulation of Magnetic Transition Temperatures Compiled by Connolly TF, Copenhaver ED (1970) Solid state literature guides. vol 5 Oak Ridge National Laboratories Literature Guides. Plenum, New York
84. Wurmehl S, Fecher GH, Kandpal HC, Ksenofonov V, Felser C, Lin HJ (2006) Investigation of Co_2FeSi: the Heusler compound with highest Curie temperature and magnetic moment. Appl Phys Lett 88:032503
85. Cable JW, Wakabayashi N, Radhakrishna P (1993) Magnetic excitations in the triangular antiferromagnets Mn_3Sn and Mn_3Ge. Phys Rev B 48:6159–6166
86. Takizawa H, Yamashita T, Uheda K, Endo T (2002) High-pressure synthesis of ferromagnetic Mn_3Ge with the Cu_3Au-type structure. J Phys Condens Matter 14:11147–11150
87. Hamaya K, Ueda K, Kishi Y, Ando Y, Sadoh T, Miyao M (2008) Epitaxial ferromagnetic Fe_3Si/Si(111) structures with high-quality heterointerfaces. Appl Phys Lett 93:132117
88. Ueda K, Hamaya K, Yamamoto K, Ando Y, Sadoh T, Maeda Y, Miyao M (2008) Low-temperature molecular beam epitaxy of a ferromagnetic full-Heusler alloy Fe_2MnSi on Ge(111). Appl Phys Lett 93:112108
89. Hamaya K, Itoh H, Nakatsuka O, Ueda K, Yamamoto K, Itakura M, Taniyama T, Ono T, Miyao M (2009) Ferromagnetism and electronic structures of nonstoichiometric Heusler-Alloy $Fe_{3-x}Mn_xSi$ epilayers grown on Ge(111). Phys Rev Lett 102:137204
90. Yamada S, Hamaya K, Yamamoto K, Murakami T, Mibu K, Miyao M (2010) Significant growth-temperature dependence of ferromagnetic properties for Co_2FeSi/Si(111) prepared by low-temperature molecular beam epitaxy. Appl Phys Lett 96:082511
91. Kasahara K, Yamamoto K, Yamada S, Murakami T, Hamaya K, Mibu K, Miyao M (2010) Highly ordered Co_2FeSi Heusler alloys grown on Ge(111) by low-temperature molecular beam epitaxy. J Appl Phys 107:09B105
92. Anumpam JPC, Rout PK, Hossain Z, Budhani RC (2010) Charge transport and magnetic ordering in laser ablated Co_2FeSi thin films epitaxially grown on (100) $SrTiO_3$. J Phys D Appl Phys 43:255002
93. Wang WH, Przybylski M, Kuch W, Chelaru LI, Wang J, Lu YF, Barthel J, Meyerheim HL, Kirschner J (2005) Magnetic properties and spin polarization of Co_2MnSi Heusler alloy thin films epitaxially grown on GaAs(001). Phys Rev B 71:144416
94. Gercsi Z, Rajanikanth A, Takahashi YK, Hono K, Kikuchi M, Tezuka N, Inomata K (2006) Spin polarization of Co2FeSi full-Heusler alloy and tunneling magnetoresistance of its magnetic tunneling junctions. Appl Phys Lett 89:082512
95. Ando Y, Hamaya K, Kasahara K, Kishi Y, Ueda K, Sawano K, Sadoh T, Miyao M (2009) Electrical injection and detection of spin-polarized electrons in silicon through an Fe_3Si/Si Schottky tunnel barrier. Appl Phys Lett 94:182105
96. Candini A, Moze O, Kockelmann W, Cadogan JM, Bruck E, Tegus O (2004) Revised magnetic phase diagram for $Fe_xMn_{5-x}Si_3$ intermetallics. J Appl Phys 95:6819–6821

97. Zeng C, Erwin SC, Feldman LC, Li AP, Jin R, Song Y, Thompson JR, Weitering HH (2003) Epitaxial ferromagnetic Mn_5Ge_3 on Ge(111). Appl Phys Lett 83:5002–5004
98. Austin AE (1969) Magnetic properties of Fe_3Ge_5-Mn_5Ge_3 solid solutions. J Appl Phys 40:1381–1382
99. Wernick JH, Wertheim GK, Sherwood SK (1972) Magnetic behavior of monosilicides of 3D-transition elements. Mater Res Bull 7:1431–1441
100. Manyala N, Sidis Y, DiTusa JF, Aeppli G, Young DP, Fisk Z (2000) Magnetoresistance from quantum interference effects in ferromagnets. Nature 404:581–584
101. Manyala N, DiTusa JF, Aeppli G, Ramirez AP (2008) Doping a semiconductor to create an unconventional metal. Nature 454:976–980
102. DiTusa JF, Friemelt K, Bucher E, Aeppli G, Ramirez AP (1997) Metal-insulator transitions in the Kondo insulator FeSi and classic semiconductors are similar. Phys Rev Lett 78:2831–2834
103. DiTusa JF, Friemelt K, Bucher E, Aeppli G, Ramirez AP (1998) Heavy fermion metal Kondo insulator transition in $FeSi_{1-x}Al_x$. Phys Rev B 58:10288–10301
104. Ishikawa Y, Tajima K, Bloch D, Roth M (1976) Helical spin structure in manganese silicide MnSi. Solid State Commun 19:525
105. Ishikawa Y, Shirane G, Tarvin JA, Kohgi M (1977) Magnetic excitations in weak itinerant ferromagnet MnSi. Phys Rev B 16:4956–4970
106. Pecheur P, Toussaint G, Kenzari H, Malaman B, Welter R (1997) Ferromagnetism of the chimney-ladder compound $Cr_{11}Ge_{19}$. J Alloy Comp 262:363–365
107. Lange H (1997) Electronic properties of semiconducting silicides. Phys Status Solidi (b) 201, 3–65 and references therein
108. Hohl H, Ramirez AP, Goldmann C, Ernst G, Bucher E (1998) Transport properties of RuSi, RuGe, OsSi, and quasi-binary alloys of these compounds. J Alloy Comp 278:39–43
109. See Madelung O (ed) (1996) Semiconductors-basic data, 2nd rev edn. Springer, Berlin
110. Lee M, Onose Y, Tokura Y, Ong NP (2007) Hidden constant in the anomalous Hall effect of high-purity magnet MnSi. Phys Rev B 75:172403
111. Lee M, Kang W, Onose Y, Tokura Y, Ong NP (2009) Unusual Hall effect anomaly in MnSi under pressure. Phys Rev Lett 102:186601
112. Neubauer A, Pfleiderer C, Ritz R, Niklowitz PG, Boni P (2009) Hall effect and magnetoresistance in MnSi. Phys B 404:3163–3166
113. Moriya T (1985) In: Fulde P (ed) Spin fluctuations in itinerant electron magnetism. Springer, Berlin
114. Pfleiderer C, Julian SR, Lonzarich GG (2001) Non-Fermi-liquid nature of the normal state of itinerant-electron ferromagnets. Nature 414:427–430
115. Pfleiderer C, Reznik D, Pintschovius L, von Lohneysen H, Garst M, Rosch A (2004) Partial order in the non-Fermi-liquid phase of MnSi. Nature 427:227–231
116. Binz B, Vishwanath A, Aji V (2006) Theory of the helical spin crystal: a candidate for the partially ordered state of MnSi. Phys Rev Lett 96:207202
117. Roβler UK, Bogdanov AN, Pfleiderer C (2006) Spontaneous skyrmion ground states in magnetic metals. Nature 442:707
118. Tewari S, Belitz D, Kirkpatrick TR (2006) Blue quantum fog: chiral condensation in quantum helimagnets. Phys Rev Lett 96:047207
119. Fischer I, Shah N, Rosch A (2008) Crystalline phases in chiral ferromagnets: destabilization of helical order. Phys Rev B 77:024415
120. Muhlbauer S, Binz B, Jonietz F, Pfleiderer C, Rosch A, Neubauer A, Georg R, Boni P (2009) Skyrmion lattice in a chiral magnet. Science 323:915–919
121. Yu XZ, Onose Y, Kanazawa N, Park JH, Han JH, Matsui Y, Nagaosa N, Tokura Y (2010) Real-space observation of a two-dimensional skyrmion crystal. Nature 465:901–904
122. Yu XZ, Kanazawa N, Onose Y, Kimoto K, Zhang WZ, Ishiwata S, Matsui Y, Tokura Y (2011) Near room-temperature formation of a skyrmion crystal in thin-films of the helimagnet FeGe. Nat Mater 10:106–109

123. Jonietz F, Muhlbauer S, Pfleiderer C, Neubauer A, Muenzer W, Bauer A, Adams T, Georgii R, Boni P, Duine RA, Everschor K, Garst M, Rosch A (2010) Spin transfer torques in MnSi at ultralow current densities. Science 330:1648–1651
124. Sato T, Sakata M (1983) Magnetic and electrical-properties of CrGe and $Cr_{11}Ge_8$. J Phys Soc Jpn 52:1807–1813
125. Richardson M (1967) Partial equilibrium diagram of Fe-Ge system in range 40–72 at. percent Ge and crystallization of some iron germanides by chemical transport reactions. Acta Chem Scand 21:2305–2317
126. Lebech B, Bernhard J, Freltoft T (1989) Magnetic-structures of cubic FeGe studied by small-angle neutron-scattering. J Phys Condens Matter 1:6105
127. Lundgren L, Beckman O, Attia V, Battacherjee SP, Richardson M (1970) Helical spin arrangement in cubic FeGe. Phys Scr 1:69–72
128. Yeo S, Nakatsuji S, Bianchi AD, Schlottmann P, Fisk Z, Balicas L, Stampe PA, Kennedy RJ (2003) First-order transition from a Kondo insulator to a ferromagnetic metal in single crystalline $FeSi_{1-x}Ge_x$. Phys Rev Lett 91:046401
129. Capan C et al To be published
130. Murarka SP (1980) Refractory silicides for integrated-circuits. J Vac Sci Technol 17:775–792
131. Murarka SP (1983) Transition-metal silicides. Annu Rev Mater Sci 13:117–137
132. Murarka SP (1995) Silicide thin-films and theor applications in microelectronics. Intermetallics 3:173–186
133. Reader AH, van Ommen AH, Weijs PJW, Wolters RAM, Oostra DJ (1993) Transition-metal silicides in silicon technology. Rep Prog Phys 56:1397–1467
134. Derrien J, Chevrier J, Le Thanh V, Crumbaker TE, Natoli JY, Berbezier I (1993) Silicide epilayers – recent developments and prospects for a Si-compatible technology. Appl Surf Sci 70(71):546–558
135. Chevrier J, Vinh LT, Derrien J (1993) Strained and relaxed semiconducting silicide layers heteroepitaxially grown on silicon. Scanning Microsc 7:473–480
136. von Kanel H, Mader KA, Muller E, Onda N, Sirringhaus S (1992) Structural and electronic-properties of metastable epitaxial FeSi1+x films on Si(111). Phys Rev B 45:R13807–R13810
137. von Kanel H, Mendik M, Mader KA, Muller E, Onda N, Goncalves-Conto S, Schwartz C, Malegori G, Miglio L, Marabelli F (1994) Elastic and vibrational properties of pseudomorphic FeSi films. Phys Rev B 50:3570–3576
138. Kafader U, Wetzel P, Pirri C, Gewinner G (1993) X-ray photoemission characterization of thin epitaxial Fe silicide phases on Si(111). Appl Phys Lett 63:2360–2362
139. Koga T, Bright A, Suzuki T, Shimada K, Tatsuoka H, Kuwara H (2000) Growth of β-$FeSi_2$ and FeSi layers by reactive deposition using Sb-related intermetallic compounds. Thin Solid Films 369:248–252
140. Matsuda K, Tatsuoka H, Matsunaga K, Isaji K, Kuwabara H, Brown PD, Xin Y, Dunn-Borkowski R, Humphreys CJ (1998) High-quality epitaxial MnSi(111) layers grown in the presence of an Sb flux. Jpn J Appl Phys 37:6556–6561
141. Matsuda K, Takano Y, Kuwabara K, Tatsuoka H, Kuwabara H, Suzuki Y, Fukuda Y, Hashimoto S, Yan Y, Pennycook SJ (2002) Formation of MnSb during the growth of MnSi layers in the presence of an Sb flux. J Appl Phys 91:4932–4935
142. Karhu E, Kahwaji S, Monchesky TL, Parsons C, Robertson MD, Maunders C (2010) Structure and magnetic properties of MnSi epitaxial thin films. Phys Rev B 82:184417
143. Karhu E, Kahwaji S, Robertson MD, Fritzche H, Kirby BJ, Majkrzak CF, Monchesky TL (2011) Helical magnetic order in MnSi thin films. Phys Rev B 84:060404(R)
144. Hortamani M, Sratskii L, Kratzer P, Mertig I (2009) Searching for Si-based spintronics by first principles calculations. New J Phys 11:125009
145. Hortamani M, Kratzer P, Scheffler M (2007) Density-functional study of Mn monosilicide on the Si(111) surface: film formation versus island nucleation. Phys Rev B 76:235426
146. Higashi S, Kocan P, Tochihara H (2009) Reactive epitaxial growth of MnSi ultrathin films on Si(111) by Mn deposition. Phys Rev B 79:205312

147. Higashi S, Ikedo Y, Kocan P, Tochihara H (2008) Epitaxially grown flat MnSi ultrathin film on Si(111). Appl Phys Lett 93:013104
148. Magnano E, Bondino F, Cepek C, Parmigiani F, Mozzati MC (2010) Ferromagnetic and ordered MnSi(111) epitaxial layers. Appl Phys Lett 96:152502
149. Magnano E, Carleschi E, Nicolaou A, Pardini T, Zagrando M, Parmigiani F (2006) Growth of manganese silicide films by co-deposition of Mn and Si on Si(111): a spectroscopic and morphological investigation. Surf Sci 600:3932–3937
150. Suto H, Imai K, Fujii S, Honda S, Katayama M (2009) Growth process and surface structure of MnSi on Si(111). Surf Sci 603:226–231
151. Schwinge K, Paggel JJ, Fumagalli P (2007) Mosaic superstructure in manganese silicide films on Si(111)-($\sqrt{3}\times\sqrt{3}$): Bi-alpha. Surf Sci 601:810–813
152. Schwinge K, Muller C, Mogilatenko A, Paggel JJ, Fumagalli P (2005) Structure and magneto-optic Kerr measurements of epitaxial MnSi films on Si(111). J Appl Phys 97:103913
153. Manyala N, Ngom BD, Beye AC, Bucher R, Maaza M, Strydom A, Forbes A, Johnson ATC, DiTusa JF (2009) Structural and magnetic properties of ε-$Fe_{1-x}Co_xSi$ thin films deposited via pulsed laser deposition. Appl Phys Lett 94:232503
154. Kulkarni JS, Kazakova O, Holmes JD (2006) Dilute magnetic semiconductor nanowires. Appl Phys A 85:277–286
155. Kazakova O, Kulkarni JS, Arnold DC, Holmes JD (2007) Engineering the magnetic properties of $Ge_{1-x}Mn_x$ nanowires. J Appl Phys 101:09H108
156. Kazakova O, Kulkarni JS, Holmes JD, Demokritov SO (2005) Room-temperature ferromagnetism in $Ge_{1-x}Mn_x$ nanowires. Phys Rev B 72:094415
157. Kazakova O, van Meulen MI, Petkov N, Holmes JD (2009) Magnetic properties of single crystalline $Ge_{1-x}Mn_x$ nanowires. IEEE Trans Magn 45:4085–4088
158. Morgunov RB, Dmitriev AI, Tanimoto Y, Kazakova O (2009) Electron spin resonance of charge carriers and antiferromagnetic clusters in $Ge_{0.99}Cr_{0.01}$ nanowires. J Appl Phys 105:093922
159. Katkar AS, Chu Y-C, Chu L-W, Chen L-J (2011) Chromium-Doped Germanium Nanotowers: Growth Mechanism and Room Temperature Ferromagnetism. Cryst Growth Des 11:2957–2963
160. Schmitt AL, Bierman MJ, Schmeisser D, Himpsel FJ, Jin S (2006) Synthesis and properties of single-crystal FeSi nanowires. Nano Lett 6:1617–1621
161. Liang S, Fang X, Xia TL, Qing YJ, Guo ZX (2010) Self-assembled magnetic nanohead-FeSi nanowire epitaxial heterojunctions by chemical vapor deposition. J Phys Chem C 114:16187–16190
162. Schmitt AL, Zhu L, Schmeisser D, Hempsel FJ, Jin S (2006) Metallic single-crystal CoSi nanowires via chemical vapor deposition of single-source precursor. J Phys Chem B 110:18142–18146
163. Seo K, Varadwaj KSK, Mohanty P, Lee S, Jo Y, Hung MH, Kim J, Kim B (2007) Magnetic properties of single-crystalline CoSi nanowires. Nano Lett 7:1240–1245
164. Schmitt AL, Higgins JM, Jin S (2008) Chemical synthesis and magnetotransport of magnetic semiconducting $Fe_{1-x}Co_xSi$ alloy nanowires. Nano Lett 8:810–815
165. In J, Varadwaj KSK, Seo K, Lee S, Jo Y, Jung MH, Kim J, Kim B (2008) Single-crystalline ferromagnetic $Fe_{1-x}Co_xSi$ nanowires. J Phys Chem C 112:4748–4752
166. Higgins JM, Ding RH, DeGrave JP, Jin S (2010) Signature of helimagnetic ordering in single-crystal MnSi nanowires. Nano Lett 10:1605–1610
167. Seo K, Yoon H, Ryu S-W, Lee S, Jo Y, Jung M-H, Kim J, Choi Y-K, Kim B (2010) Itinerant helimagnetic single-crystalline MnSi nanowires. ACS Nano 4:2569–2576
168. Schmitt AL, Higgins JM, Szczech JR, Jin S (2010) Synthesis and applications of metal silicide nanowires. J Mater Chem 20:223–235
169. Song YP, Schmitt AL, Jin S (2007) Ultralong single-crystal metallic Ni_2Si nanowires with low resistivity. Nano Lett 7:965–969

170. Higgins JM, Carmichael P, Schmitt AL, Lee S, Degrave JP, Jin S (2011) Mechanistic investigation of the growth of $Fe_{1-x}Co_xSi$ ($0 \leq x \leq 1$) and $Fe_5(Si_{1-y}Ge_y)_3$ ($0 \leq y \leq 0.33$) ternary alloy nanowires. ACS Nano 5:3268–3277
171. Higgins JM, Ding RH, Jin S (2011) Synthesis and characterization of manganese-rich silicide α-Mn_5Si_3, β-Mn_5Si_3, and β -Mn_3Si nanowires. Chem Mater 23:3848–3853
172. Szczech JR, Schmitt AL, Bierman MJ, Jin S (2007) Single-crystal semiconducting chromium disilicide nanowires synthesized via chemical vapor transport. Chem Mater 19:3238–3243
173. Seo K, Varadwaj KSK, Cha D, In J, Kim J, Park J, Kim B (2007) Synthesis and electrical properties of single crystalline $CrSi_2$ nanowires. J Phys Chem C 111:9072–9076
174. DeGrave JP, Schmitt AL, Selinsky RS, Higgins JM, Keavney DJ, Jin S (2011) Spin polarization measurement of homogeneously doped $Fe_{1-x}Co_xSi$ nanowires by Andreev reflection spectroscopy. Nano Lett 11:4431–4437
175. Hung S-W, Wang TT-J, Chu L-W, Chen L-J (2011) Orientation-dependent room-temperature ferromagnetism of FeSi nanowires and applications in nonvolatile memory devices. J Phys Chem C 115:15592–15597
176. Liu H, She GW, Ling ST, Mu LX, Shi WS (2011) Ferromagnetic Si/$Mn_{27}Si_{47}$ core/shell nanowire arrays. J Appl Phys 109:044305
177. Zeng CG, Kent PRC, Varela M, Eisenbach M, Stocks GM, Torija M, Shen J, Weitering HH (2006) Epitaxial stabilization of ferromagnetism in the nanophase of FeGe. Phys Rev Lett 96:127201
178. Yan CY, Higgins JM, Faber MS, Lee PS, Jin S (2011) Spontaneous growth and phase transformation of highly conductive nickel germanide nanowires. ACS Nano 5:5006–5014
179. Theodoropoulou N, Hebard AF, Chu SNG, Overberg ME, Abernathy CR, Pearton SJ, Wilson RG, Zavada JM, Park YD (2002) Magnetic and structural properties of Fe, Ni, and Mn-implanted SiC. J Vac Sci Technol A 20:579–582
180. Stromberg F, Keune W, Chen X, Bedanta S, Reuther H, Muncklich A (2006) The origin of ferromagnetism in Fe-57 ion-implanted semiconducting 6H-polytype silicon carbide. J Phys Condens Mater 18:9881–9900
181. Song B, Bao HQ, Li H, Lei M, Peng TH, Jian JK, Liu J, Wang WY, Wang WJ, Chen XL (2009) Observation of glassy ferromagnetism in Al-doped 4H-SiC. J Am Chem Soc 131:1376–1377
182. Ma SB, Sun YP, Zhao BC, Tong P, Zhu XB, Song WH (2007) Magnetic properties of Mn-doped cubic silicon carbide. Phys B 394:122–126
183. Song B, Bao HQ, Li H, Lei M, Jian JK, Han JC, Zhang XH, Meng SH, Wang WY, Chen XL (2009) Magnetic properties of Mn-doped 6H-SiC. Appl Phys Lett 94:102508
184. Song B, Chen XL, Han JC, Wang G, Bao HQ, Duan LB, Zhu KX, Li H, Zhang ZH, Wang WY, Zhang XH, Meng SH (2011) Raman scattering and magnetizations studies of (Al, Cr)-codoped 4H-SiC. J Magn Magn Matter 323:2876–2882
185. Seong HK, Park TE, Lee SC, Lee KR, Park JK, Choi HJ (2009) Magnetic properties of vanadium-doped silicon carbide nanowires. Met Mater Int 15:107–111
186. Shaposhnikov VL, Sobolev NA (2004) The electronic structure and magnetic properties of transition metal-doped silicon carbide. J Phys Condens Matter 16:1761–1768
187. Los A, Los V (2010) Room temperature ferromagnetism in Mn-doped silicon carbide from first-principles calculations. J Phys Condens Matter 22:245801

Further Reading

Bader SD (2006) Colloquium: opportunities in nanomagnetism. Rev Mod Phys 78:1–15
Choi HJ, Seong HK, Kim U (2008) Diluted magnetic semiconductor nanowires. Nano 3:1–19
Dietl T, Ohno H (2006) Engineering magnetism in semiconductors. Matter Today 9:18–26
Fabian J, Matos-Abiague A, Ertler C, Stano P, Zutic I (2007) Semiconductor spintronics. Acta Phys Slov 57:565–907

Hanson R, Awschalom DD (2008) Coherent manipulation of single spins in semiconductors. Nature 453:7198

Krishnan KM, Pakhomov AB, Bao Y, Blomqvist P, Chun Y, Gonzales M, Griffin K, Ji X, Roberts BKN (2006) Nanomagnetism and spin electronics: materials, microstructure and novel properties. J Matter Sci 41:793–815

Maekawa S (ed) (2006) Concepts in spin electronics. Oxford University Press, Oxford

Macdonald AH, Schiffer P, Samarth N (2005) Ferromagnetic semiconductors: moving beyond (Ga, Mn)As. Nat Mater 4:195–202

Schliemann J (2006) Spin hall effect. Int J Mod Phys B 20:1015–1036

Valenzuela SO (2009) Nonlocal electronic spin detection, spin accumulation and the spin hall effect. Int J Mod Phys 23:2413–2438

Von Molnar S, Read D (2002) Magneto-transport in magnetic compound semiconductors and metals. J Magn Magn Mater 242:13–20

Von Molnar S, Read D (2003) New materials for semiconductor spin-electronics. Proc IEEE 91:715–726

Wolf SA, Awschalom DD, Buhrman RA, Daughton JM, von Molnar S, Roukes ML, Chtchelkanova AY, Treger DM (2001) Spintronics: a spin-based electronics vision for the future. Science 294:1488–1495

Wu H, Kratzer P, Scheffler M (2007) Density-functional theory study of half-metallic heterostructures: interstitial Mn in Si. Phys Rev Lett 98:117202

Wu MW, Jiang JH, Weng MQ (2010) Spin dynamics in semiconductors. Phys Rep Rev Sec Phys Lett 493:61–236

Zutic I, Dery H (2011) Spintronics: taming spin currents. Nat Mater 10:646–647

Zutic I, Fabian J, Das Sarma S (2004) Spintronics: fundamentals and applications. Re Mod Phys 76:323–410